Cell

Viral DNA polymerase structures reveal mechanisms of antiviral drug resistance

Graphical abstract

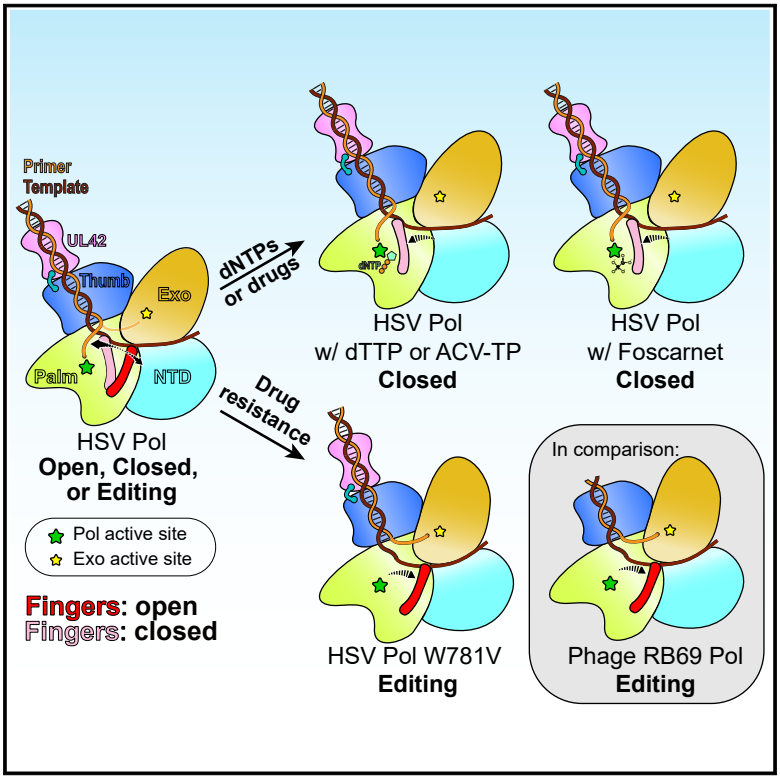

Authors

Sundaresh Shankar, Junhua Pan, Pan Yang, ..., Mrinal Shekhar, Donald M. Coen, Jonathan Abraham

Correspondence

jonathan_abraham@hms.harvard.edu

In brief

High-resolution cryo-EM structures of a fully assembled DNA- and drug-bound herpes simplex virus polymerase holoenzyme complex, in a number of conformations, characterize the mechanisms that drive drug selectivity and resistance profiles of this DNA polymerase.

Highlights

- Cryo-EM structures reveal how HSV polymerase interacts with DNA and antivirals
- Polymerase is in multiple conformations when not bound to nucleotide or antiviral
- Antiviral resistance mutations alter polymerase conformational dynamics

Shankar et al., 2024, Cell *187*, 1–15
October 3, 2024
https://doi.org/10.1016/j.cell.2024.07.048

CellPress

Please cite this article in press as: Shankar et al., Viral DNA polymerase structures reveal mechanisms of antiviral drug resistance, Cell (2024), https://doi.org/10.1016/j.cell.2024.07.048

Cell

CellPress
OPEN ACCESS

Article

Viral DNA polymerase structures reveal mechanisms of antiviral drug resistance

Sundaresh Shankar,[1,9] Junhua Pan,[1,2,9] Pan Yang,[1,9] Yuemin Bian,[3,4,9] Gábor Oroszlán,[1,5] Zishuo Yu,[1] Purba Mukherjee,[5,6] David J. Filman,[5] James M. Hogle,[5] Mrinal Shekhar,[4] Donald M. Coen,[5] and Jonathan Abraham[1,7,8,10,*]

[1]Department of Microbiology, Blavatnik Institute, Harvard Medical School, Boston, MA 02115, USA
[2]Biomedical Research Institute and School of Life and Health Sciences, Hubei University of Technology, Wuhan, Hubei, China
[3]School of Medicine, Shanghai University, Shanghai, China
[4]Center for the Development of Therapeutics, Broad Institute of Harvard and MIT, Cambridge, MA 02142, USA
[5]Department of Biological Chemistry and Molecular Pharmacology, Blavatnik Institute, Harvard Medical School, Boston, MA 02115, USA
[6]York Structural Biology Laboratory, Department of Chemistry, University of York, Heslington, York, UK
[7]Department of Medicine, Division of Infectious Diseases, Brigham and Women's Hospital, Boston, MA 02115, USA
[8]Center for Integrated Solutions in Infectious Diseases, Broad Institute of Harvard and MIT, Cambridge, MA 02142, USA
[9]These authors contributed equally
[10]Lead contact
*Correspondence: jonathan_abraham@hms.harvard.edu
https://doi.org/10.1016/j.cell.2024.07.048

SUMMARY

DNA polymerases are important drug targets, and many structural studies have captured them in distinct conformations. However, a detailed understanding of the impact of polymerase conformational dynamics on drug resistance is lacking. We determined cryoelectron microscopy (cryo-EM) structures of DNA-bound herpes simplex virus polymerase holoenzyme in multiple conformations and interacting with antivirals in clinical use. These structures reveal how the catalytic subunit Pol and the processivity factor UL42 bind DNA to promote processive DNA synthesis. Unexpectedly, in the absence of an incoming nucleotide, we observed Pol in multiple conformations with the closed state sampled by the fingers domain. Drug-bound structures reveal how antivirals may selectively bind enzymes that more readily adopt the closed conformation. Molecular dynamics simulations and the cryo-EM structure of a drug-resistant mutant indicate that some resistance mutations modulate conformational dynamics rather than directly impacting drug binding, thus clarifying mechanisms that drive drug selectivity.

INTRODUCTION

Although much is known about the structures of family B DNA polymerases, which include eukaryotic DNA polymerases α, δ, and ε, a better understanding of their conformational dynamics is a critical missing link between their structures and function. Viral family B DNA polymerases are major targets for antivirals, including agents that are active against poxviruses, adenoviruses, and herpesviruses.[1] The herpes simplex virus (HSV) polymerase is the target of the triphosphate (TP) form of the nucleoside analog acyclovir (ACV), the leading antiviral drug for treating HSV infection, and of foscarnet, a pyrophosphate analog that is a second-line drug. For both antivirals, substitutions in numerous locations in the catalytic subunit of the polymerase (UL30 or Pol) can cause clinically relevant resistance (reviewed in Piret and Boivin).[2] How these mutations confer resistance and why ACV and foscarnet are selective against herpesvirus polymerases is poorly understood.

The HSV polymerase is a heterodimer of Pol and a processivity subunit (UL42) that promotes long-chain DNA synthesis.[3] HSV Pol has characteristic thumb, palm, and fingers domains, a 3′–5′ exonuclease domain (Exo), and an NH_2-terminal domain (NTD). Pol also has a herpesvirus-specific pre-NH_2 domain of unknown function.[4] UL42 resembles a monomer of the eukaryotic sliding clamp protein proliferating cell nuclear antigen (PCNA).[5] However, UL42 binds DNA tightly as a monomer instead of being loaded as a trimeric ring around DNA like PCNA.[5–11] How Pol and UL42 bind DNA tightly yet rapidly and processively synthesize DNA remains unclear.[6,11,12] X-ray crystal structures of Pol alone and of UL42 bound to a Pol C-terminal peptide were previously available, and an X-ray crystal structure of HSV Pol bound to DNA primer template and a non-nucleoside analog was recently described.[4,5,13]

Here, we used cryo-electron microscopy (cryo-EM) to obtain several high-resolution structures of the HSV Pol-UL42 heterodimer bound to DNA primer-template in the absence or presence of an incoming nucleotide or antiviral drug. The DNA-bound

Please cite this article in press as: Shankar et al., Viral DNA polymerase structures reveal mechanisms of antiviral drug resistance, Cell (2024), https://doi.org/10.1016/j.cell.2024.07.048

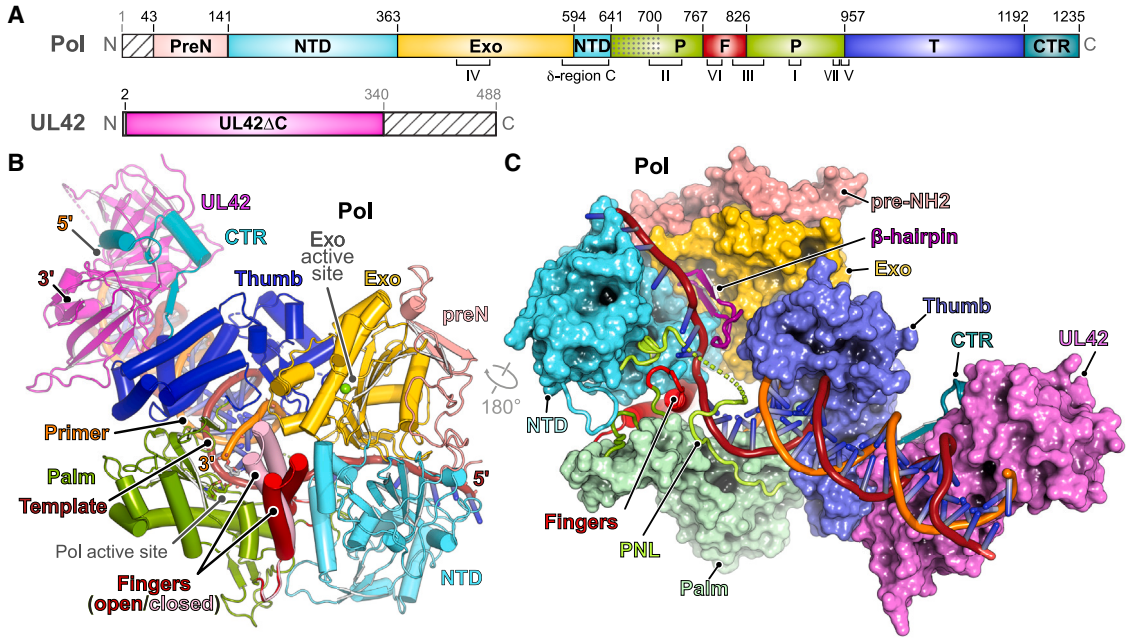

Figure 1. Structure of the DNA-bound HSV polymerase holoenzyme

(A) Diagrams of HSV Pol and UL42 constructs used for structural studies. Pol conserved regions (CR) I–VII are shown in brackets. δ-region C[14] is also indicated. Stripes indicate regions not included in constructs. preN, pre-NH2; NTD, NH2-terminal domain; Exo, exonuclease domain; P, palm; F, fingers; T, thumb; CTR, C-terminal region. The dotted segment indicates the palm-NTD loop.

(B) DNA-bound HSV polymerase in the absence of nucleotide. The primer 3′ end is in the Pol active site. We observed alternate conformations for the fingers (open and closed) (see Figure S1D).

(C) Surface representation of DNA-bound HSV polymerase in a rotated view. The fingers, loops near the base of the fingers, palm-NTD loop, Exo β-hairpin motif, Pol CTR, and DNA are shown as ribbons.

See also Figure S1.

polymerase samples the open, closed, and editing conformations as it awaits a substrate. Structural analyses paired with molecular dynamics (MD) simulations suggest that several mutations that are distant from the sites of drug binding confer antiviral resistance by influencing fingers domain dynamics. The structures also reveal how Pol and UL42 interact with DNA, with implications for the mechanism of processive DNA synthesis.

RESULTS

Overall structure of the DNA-bound HSV Pol-UL42 heterodimer

We expressed HSV Pol (residues 43–1,235) in insect cells and UL42 (residues 2–340) in bacterial cells and confirmed that the proteins were active in a DNA elongation assay (Figures 1A and S1A). We assembled Pol and UL42 onto a DNA primer-template (PT1) (Figure S1B) in the absence of nucleotide and visualized complexes by single-particle cryo-EM (Figure S1C). Particles from the most prominent 3D class yielded a map with a global resolution of 2.7 Å (Figure S1C). The local resolution is highest near the Pol active site and lower for the Pol C-terminal region (CTR) and UL42, likely due to flexibility in these regions.

As in the structures of other DNA-bound family B polymerases, HSV Pol resembles a hand gripping the double-stranded (ds) portion of the DNA primer-template (Figures 1B and 1C). Pol's CTR extends from the thumb to interact with UL42. The overall mode of primer-template binding and residues that mediate key contacts with DNA are generally conserved with other B-family DNA polymerases. These include prominent contacts made by conserved region (CR) VII and CRV in the Pol palm and thumb, respectively (Figures S2A, S2B, and S2C). The 5′ end of the primer in the ds portion of the primer-template begins at one end of UL42 and extends along the processivity factor and then along the Pol thumb where the 3′ end of the primer enters the Pol active site between the thumb, palm, and fingers (Figure 1C). The transition between ds and single-stranded (ss) DNA occurs at the active site, with the ssDNA template strand bending away from the active site and accessing a groove between the Exo and NTD (Figure 1C). We observed strong density for the first three nucleotides in the ssDNA binding groove, as seen in other structures of family B polymerases.[15,16] As in some other B-family Pols (e.g., Pol δ and bacteriophage RB69 Pol), a β-hairpin motif in Exo provides contacts that stabilize the ssDNA (Figure 1C).[17]

HSV Pol palm-NTD loop DNA contacts

A sixty-residue segment that is near the junction of the palm and the NTD (residues 641–700), referred to here as the "palm-NTD loop," was disordered in the apo-HSV Pol structure.[4] Sequence alignments suggest that only certain α- and β-herpesvirus Pols have such a long palm-NTD loop (Data S1). In HSV Pol and several other α-herpesviruses, the loop is rich in charged amino

Please cite this article in press as: Shankar et al., Viral DNA polymerase structures reveal mechanisms of antiviral drug resistance, Cell (2024), https://doi.org/10.1016/j.cell.2024.07.048

CellPress
OPEN ACCESS

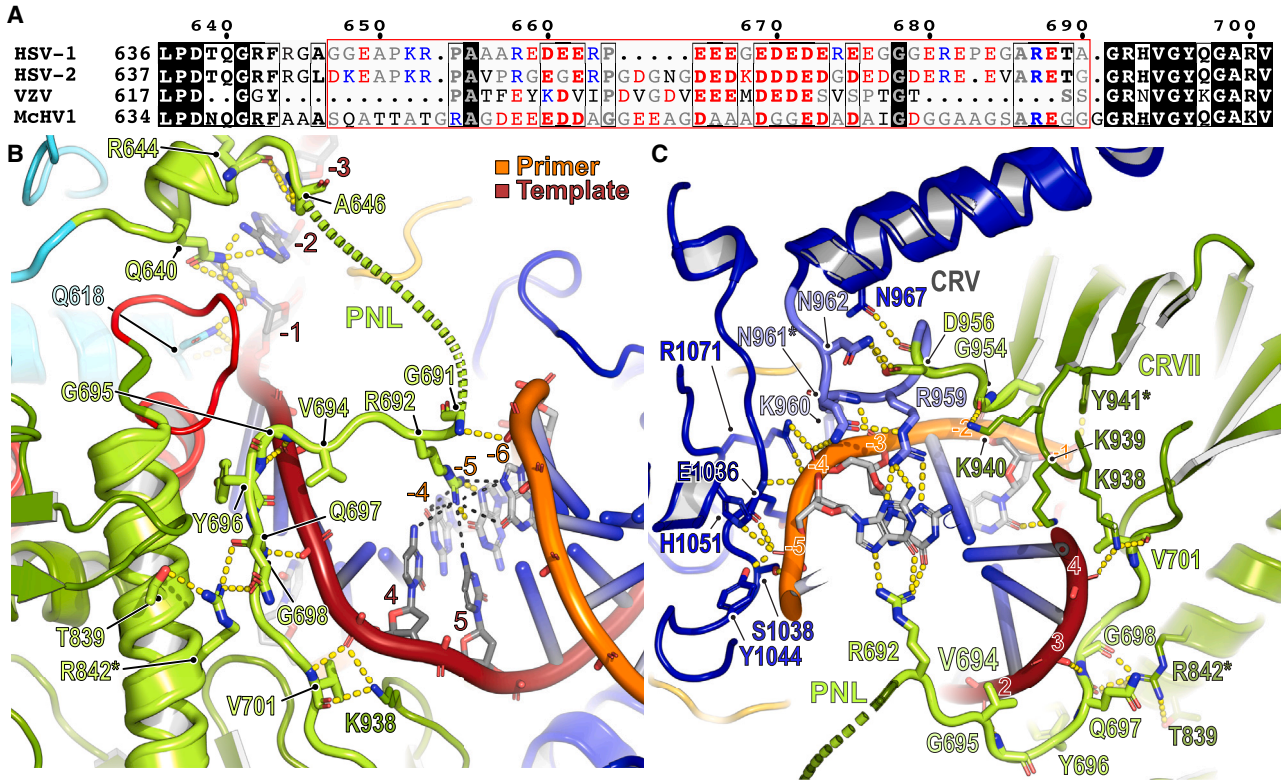

Figure 2. HSV Pol palm, palm-NTD loop, and thumb DNA contacts

(A) Sequence alignment showing the palm-NTD loop (PNL) region (residues 641–700). Red box indicates residues that are disordered in the structure. Within the red box, positively and negatively charged residues are colored in blue and red, respectively; residues with linker-like properties (serine, alanine, glycine, and proline) are in gray. McHV1, Macacine herpesvirus 1; VZV, varicella zoster virus. Alignment was generated using ESPript 3.0.[18]

(B) PNL DNA contacts for the nucleotide-free polymerase (open conformation). The polar contacts that the $R692_{Pol}$ side chain makes with the primer −5 base from the primer 3′ end are shown as yellow dashes, and other contacts with neighboring bases are shown as thin black dashes. Additional side chain and protein backbone contacts involving Pol residues in this region are shown as yellow dashes.

(C) Pol palm, thumb, and PNL contacts with DNA for the closed (dTTP-bound) polymerase. CRV and CRVII engage the primer near its 3′ end, and the PNL engages the backbone of the DNA template on the opposite side of the duplex. Selected contacts are shown, with polar contacts shown as yellow dashes. See also Figure S2.

In (B) and (C), $R842_{Pol}$, $Y941_{Pol}$, and $N961_{Pol}$, indicated by asterisks, are sites of mutations that confer associated with antiviral resistance (see text). See also Figure S2.

acids (mostly glutamates) and small amino acids that likely make it flexible (Figure 2A). Residues 641–646 and 691–700 can be visualized in the structure, while residues 647–690 remain disordered (Figures 2A and 2B).

On the NTD side of the loop, $Q640_{Pol}$ stabilizes nucleotide residue −1 of the ss template by forming a pseudo base pair and stabilizes template nucleotide residue −2 through additional contacts (Figure 2B). On the palm side of the loop, the $R692_{Pol}$ side chain makes extensive polar contacts with the bases of both the template (+4 and +5 positions) and primer (−4, −5, and −6 positions) (Figure 2B). The side chains of $V694_{Pol}$ and $Y696_{Pol}$ grasp the DNA backbone of template residues +1 and +2, and the main chain amides of $G695_{Pol}$ and $G698_{Pol}$ interact with the DNA backbone of the template (Figure 2B). Most of the palm-NTD loop contacts with DNA are like those described in the X-ray crystal structure of DNA-bound HSV Pol in the presence of a non-nucleoside inhibitor.[13] However, in that prior structure, $R692_{Pol}$ was only visible in one of the two copies in the asymmetric unit of the crystal, and the arginine side chain was observed contacting bases on the template strand only.[13] Thus, the position of $R692_{Pol}$ may change as Pol monitors the geometry of the primer and template strands.

There is substantial divergence in the Pol segments that contact DNA in other B-family Pols in the region where the palm-NTD loop contacts DNA (Figures S2C–S2F). For example, in RB69 and human Pol δ, some of the contacts are made by segments of the palm and Exo domains (Figures S2D and S2E).[15,19] In yeast Pol ε, the analogous region contains a subdomain that involves different palm loops and wraps around DNA (Figure S2F).[20] Pol α makes contacts that are most like those of HSV Pol, with palm residue R834, like HSV $R692_{Pol}$, interacting with both the DNA primer and template strands (Figures S2G and S2H).[21] Although most of the HSV Pol palm-NTD loop remains disordered in the structure, the visualized segments may play an important role in sensing primer-template geometry during DNA replication.

Please cite this article in press as: Shankar et al., Viral DNA polymerase structures reveal mechanisms of antiviral drug resistance, Cell (2024), https://doi.org/10.1016/j.cell.2024.07.048

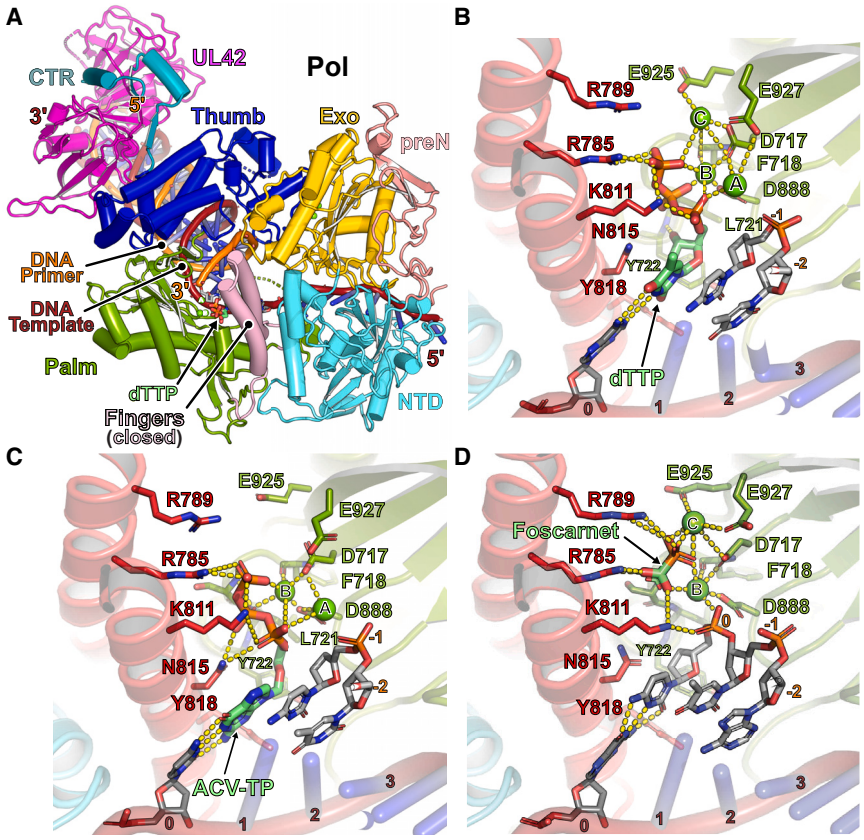

Figure 3. DNA-bound HSV polymerase in the closed conformation and active site recognition of nucleotide or antivirals

(A) HSV polymerase in the closed conformation bound to DNA primer template with deoxythymidine triphosphate (dTTP) opposite the templating base. dTTP is shown as sticks.

(B) HSV Pol active site with dTTP.

(C) HSV Pol active site with acyclovir triphosphate (ACV-TP).

(D) HSV Pol active site with foscarnet. The primer 3′ end is untranslocated.

The complexes included a 3′-dideoxy-terminated primer to prevent nucleotide incorporation. Metals are shown as green spheres. In (B)–(D), selected contacts are shown as yellow dashes.

See also Figure S3.

HSV Pol samples multiple conformations in the absence of nucleotide

Unexpectedly, high-resolution maps of the DNA-bound holoenzyme free of dNTPs after 3D classification and refinement revealed both the open and closed conformation of the fingers domain; in final maps, the density associated with each conformation, contoured at the same level, is of comparable strength and quality (Figure S1D). These features suggest that the polymerase fingers open and close toward the palm active site even in the absence of a nucleotide substrate. Indeed, 3D variability analysis[22] of this dataset revealed fingers opening and closing toward the enzyme active site (Video S1). Conformational sampling by the fingers in the absence of a nucleotide in the active site explains how DNA binding alone alters the protease sensitivity of the HSV Pol NTD region (δ region C) that packs against the fingers.[23]

Furthermore, examination of volumes obtained at the 3D classification stage revealed a subclass of particles (roughly 30%) in which the 3′ end of the primer was oriented toward the Exo active site, thus likely representing the editing conformation, with maps to 3.8 Å resolution (Figure S1C). These observations indicate that DNA-bound HSV polymerase readily adopts the open, closed, and editing conformations in the absence of a nucleotide in the active site.

Mode of nucleotide binding in the active site

We added deoxythymidine TP (dTTP) to HSV polymerase assembled on DNA PT1 to determine a 2.8 Å resolution structure of a closed holoenzyme (Figures 3A and S3A). We observed density for the nucleotide and three metals in the active site (A, B, and C, with metal C showing the weakest density) (Figures 3B and S3F). We did not observe density for open fingers, indicating that addition of dTTP completely shifted the fingers toward a closed conformation. Fingers residues $R785_{Pol}$ and $K811_{Pol}$ interact with the phosphates of the incoming nucleotide, and the $N815_{Pol}$ side chain interacts with the base (within 4 Å) (Figure 3B). The nucleotide, side chains of $D717_{Pol}$, $D888_{Pol}$, $E925_{Pol}$, $E927_{Pol}$, and the $F718_{Pol}$ backbone carbonyl in the palm together coordinate metal ions in the active site (Figure 3B). Palm residues $L721_{Pol}$ and $Y722_{Pol}$ interact with the ribose of the incoming nucleotide. The side chain of $Y722_{Pol}$ is positioned to serve its expected role as a steric gate for ribonucleotide exclusion, and the side chain of $Y818_{Pol}$ is positioned to ensure proper nucleotide incorporation by preventing protrusion of mismatched nascent base pairs. Most of these interactions are well conserved in family B DNA polymerases and were previously predicted from the apo-HSV Pol structure.[4]

Incoming ACV-TP makes weaker contacts to stabilize a closed Pol

ACV is a guanosine analog that lacks 2′ and 3′ hydroxyl moieties and requires activation by a viral thymidine kinase. The TP form of ACV (ACV-TP) competitively inhibits Pol, and ACV-TP incorporation into growing DNA results in chain termination.[24,25] We added ACV-TP to polymerase assembled onto a DNAprimer-template designed to accommodate the drug opposite a templating cytosine (PT2) and determined the 2.8 Å cryo-EM structure of a closed, drug-bound complex (Figures 3C, S1B, and S3B). There was no evidence of open fingers, and only metals A and B had clear features in cryo-EM maps (Figures 3C and S3G). The binding modes of dTTP and ACV-TP are similar, except that the $N815_{Pol}$ side chain makes polar contacts with the ACV-TP α- and β-phosphates in addition to interacting with

Please cite this article in press as: Shankar et al., Viral DNA polymerase structures reveal mechanisms of antiviral drug resistance, Cell (2024), https://doi.org/10.1016/j.cell.2024.07.048

the base (Figure 3C). Because ACV lacks 2′ and 3′ moieties, prominent hydrophobic interactions of the $Y722_{Pol}$ side chain with the ribose ring and a strong (<3 Å) polar contact the 3′ hydroxyl of dTTP makes with the $L721_{Pol}$ backbone amide are lost (Figures 3B and 3C). ACV-TP would thus make weaker contacts to stabilize the closed state as compared with incoming nucleotides, consistent with HSV Pol's higher apparent K_m for ACV-TP than for nucleotide.[26]

Foscarnet favors a closed, untranslocated polymerase complex

Foscarnet is a pyrophosphate analog that can be used to treat infection by certain ACV-resistant strains of HSV (e.g., HSV strains that lack thymidine kinase).[1,27] We added foscarnet to polymerase assembled onto a DNA PT (PT1) and determined a 3.3 Å cryo-EM structure of a foscarnet-bound complex (Figures S1B and S3C). The foscarnet-bound polymerase was mainly in the closed, untranslocated state, with the 3′ end of the primer still in the Pol active site (Figure 3D). From the fingers, $R785_{Pol}$, which contacts the γ-phosphate of dTTP and ACV-TP, binds the foscarnet carbonyl group. $K811_{Pol}$, which interacts with the phosphates of dTTP and ACV-TP, instead contacts both the carbonyl group of foscarnet and the phosphate of the untranslocated primer 3′ end (Figure 3D). $R789_{Pol}$, a well-conserved basic residue (Data S1) that does not contact the phosphates of dTTP or ACV-TP, interacts with the phosphonate moiety of foscarnet (Figures 3B–3D). Metals B and C interact with both the carbonyl and phosphonate moieties of foscarnet and likely impose geometric constraints on drug positioning (Figure 3D). The structure of the foscarnet-bound polymerase possibly reflects the configuration of the active site following phosphoryl transfer, before the pyrophosphate group exits the active site.

Interestingly, we also observed weak density for open polymerase fingers in maps of the foscarnet-bound complex (Figure S3D), and density for the terminal nucleotide of the untranslocated primer was also weaker than expected as compared with that of the dTTP-occupied active site. This observation suggests that at the concentration of foscarnet we used (equimolar with the DNA-bound polymerase complex), the enzyme is in an equilibrium between drug-bound untranslocated and drug-free translocated states and between having closed and open fingers, with foscarnet favoring the closed, untranslocated state.

Drug-resistance mutations

Polymerase substitutions that render HSV polymerase resistant to ACV and/or to pyrophosphate analogs such as foscarnet and its close analog phosphonoacetic acid are found at multiple locations in Pol (Figure 4A). For ACV resistance, one of these substitutions, N815S,[28,29] affects a residue whose side chain makes a polar contact with ACV-TP that it does not make with dTTP (Figures 3B and 3C). Based on its location, this mutation would not be expected to affect foscarnet binding (Figure 3D), consistent with the known foscarnet sensitivity of HSV containing the N815S mutation (Table 1).[28,29,37] Thus, the N815S mutation appears to directly affect ACV-TP binding. However, unlike N815S, most resistance substitutions are relatively distant from the sites of drug binding in the Pol active site (Figure 4A).

Substitutions predicted to influence fingers domain dynamics

We next turned to MD simulations to evaluate resistance substitutions that may affect the dynamics of the fingers domain based on their positions at interdomain interfaces. With the cryo-EM structures as starting points, we used root-mean-square-fluctuation (RMSF) calculations derived from MD simulations to compare structural fluctuations at each Pol residue position between wild-type (WT) and mutant proteins for both open and closed (with dTTP present) conformations. For each mutant, the relevant residue was substituted *in silico* in both the open and closed structures, followed by an energy minimization step prior to the MD simulation. This approach allowed us to model mutated interfaces.

The W781V Pol mutation in the fingers domain causes ACV and foscarnet resistance (Table 1).[36] W781V had previously been hypothesized to cause foscarnet resistance by shifting the conformational equilibrium of the fingers domain toward the open conformation.[36] RMSF calculations revealed that W781V increases structural fluctuation of the fingers in both the open and closed Pol conformations (Figures 4B–4D). $W781_{Pol}$ is at the interface of the fingers and NTD, where its side chain makes hydrophobic interactions with surrounding leucines or valines in both the open and closed Pol conformations (Figure 4E). W781V would remove these hydrophobic interactions in both the open and closed Pol conformations (Figure 4F), thus explaining the increased structural fluctuations observed in both conformations. The increases in structural fluctuations caused by the mutation are less prominent in the closed Pol conformation probably because nucleotide stabilizes the closed conformation, as demonstrated through RMSF calculations performed with and without dTTP for the WT and W781V mutant enzymes (Figures 4G, 4H, and S4A).

We carried out similar analyses for three additional Pol mutations that are at interfaces between the fingers domain and other Pol domains and cause ACV and foscarnet resistance—A605V, E597K, and L774F. The A605V substitution is in NTD δ-region C and causes resistance to ACV and foscarnet (Table 1).[30,33] A605V, like W781V, increased RMSF fluctuations of the fingers domain in both the open and closed conformations (Figures S4B and S5A). $A605_{Pol}$ faces the W781 side chain in the closed but not open Pol conformation (Figure S5B). MD simulations suggest that the presence of the larger valine side chain on the NTD facing the W781 side chain may sterically hinder closure of the fingers (Figure S5C). Furthermore, MD analysis suggests that the effects of A605V in the open polymerase likely involve conformational changes in the side chains of neighboring residues, including $A600_{Pol}$ on the NTD and $A809_{Pol}$ in the fingers domain, resulting in steric hindrance (Figure S5C).

The E597K mutation, which is also within NTD δ-region C, confers resistance to ACV and the pyrophosphate analog phosphonoacetic acid (Table 1).[30,31] E597K increases fluctuations of the fingers domain in both the open and closed conformations (Figures S4C and S5D). $E597_{Pol}$ is in a region where the NTD, fingers, and Exo domains meet (Figure S5E). E597K would disrupt salt bridges with residue $K532_{Pol}$ in the Exo domain in both the open and closed conformations (Figure S5F), explaining its effect of increasing structural fluctuations in both conformations.

Please cite this article in press as: Shankar et al., Viral DNA polymerase structures reveal mechanisms of antiviral drug resistance, Cell (2024), https://doi.org/10.1016/j.cell.2024.07.048

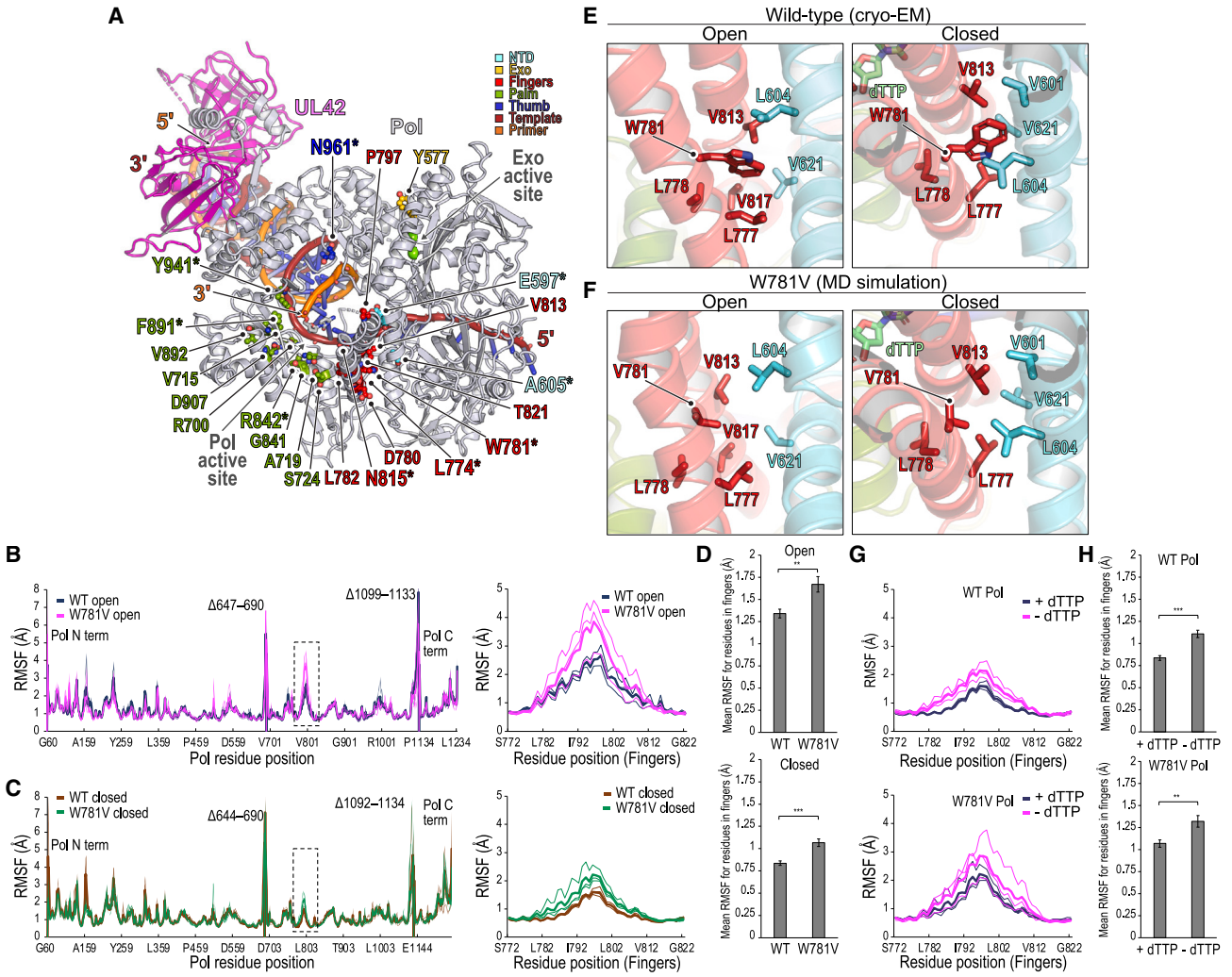

Figure 4. Drug-resistance mutations influence polymerase fingers dynamics

(A) Substitutions that confer resistance to acyclovir and/or a pyrophosphate analog as demonstrated by genetic experiments such as marker transfer are mapped on DNA-bound HSV polymerase in the open conformation. Substituted residues are shown as sticks and colored according to domains. Residues labeled with asterisks are discussed in the text. Substitutions and their effects on drug resistance are reviewed in Piret and Boivin.[2]

(B and C) Per-residue root-mean-square-fluctuation (RMSF) from MD simulations of the polymerase in the open conformation for wild-type (WT) (blue trace) and the W781V mutant (pink trace) (B), or of the polymerase in the closed conformation for the WT (brown trace) and the W781V mutant (green trace) (C).

(D) Mean RMSF values calculated during MD simulations for fingers residues (S772–G822) are plotted for the WT (cryo-EM) and W781V (modeled) structures in the open (top) and closed (bottom) conformations.

(E) View of fingers domain residue W781 and neighboring hydrophobic residues in the open and closed (dTTP-bound) conformations in the cryo-EM structures.

(F) View of representative frames from MD simulations to show neighboring hydrophobic residues for the W781V mutant enzyme in the open and closed conformations.

(G) Per-residue fluctuation from MD simulations of the holoenzyme in the closed conformation for the WT holoenzyme (top) or W781V Pol mutant (bottom) in the presence or absence of dTTP. Only the fingers residues are shown.

(H) Mean RMSF values calculated during MD simulations for fingers residues (S772–G822) are plotted for the WT (top) and W781V mutant (bottom) in the closed conformation.

For (B) and (C), the right panels show plots of the fingers region, indicated by the dashed box in the left panels. Regions denoted "Δ" are absent in models (lacked interpretable density in cryo-EM maps). For panels in (G), full tracings are provided in Figure S4. For (D) and (H), comparison between two groups was performed using an unpaired, two-tailed Student's t test. Error bars represent standard errors. $^{**}p < 0.01$, $^{***}p < 0.001$.

See also Figures S4, S5, and S6.

Unlike the other mutations we examined, the L774F drug-resistance mutation (Table 1)[35] increased structural fluctuations of the fingers domain only in the closed Pol conformation, where the effect was relatively modest but statistically significant (Figures S4D and S5G). $L774_{Pol}$ is at the base of the fingers, where it occupies a hydrophobic pocket that involves other residues from the adjacent fingers helix, the palm, and the NTD in both the open and closed conformations (Figure S5H). Distances

Please cite this article in press as: Shankar et al., Viral DNA polymerase structures reveal mechanisms of antiviral drug resistance, Cell (2024), https://doi.org/10.1016/j.cell.2024.07.048

CellPress
OPEN ACCESS

Table 1. Summary of resistance profiles and Pol activity assays for drug-resistant mutants analyzed in this study

Mutant	Effects	ACV with virus	Foscarnet (PFA) and/or PAA[a] with virus	Aph. w/virus	Enzymatic apparent kinetic constants	Fidelity	References
E597K	increased structural fluctuations open/closed	r (3×)	r (PAA)[a] (2×)	N/A	ACV-TP K_m (4.7×), k_{cat} (0.35×), K_i (4.1×)	N/A	Huang et al.,[26] Gibbs et al.,[30] Coen et al.,[31] and Chiou[32]
A605V	increased structural fluctuations open/closed	r (5×)	r[b] (>8×)	hs (0.1×)	ACV-TP K_m (1.4×), k_{cat} (0.049×), K_i (3.5×) PFA K_i (23×)	N/A	Huang et al.,[26] Gibbs et al.,[30] Chiou,[32] Saijo et al.,[33] and Bastow et al.[34]
L774F	increased structural fluctuations, closed only	r (4×)	r (3×)	hs (0.7×)	N/A	increased	Hwang et al.[35,38]
W781V	increased structural fluctuations open/closed; cryo-EM structure favors the editing conformation	r (14×)	r (3×)	N/A	PFA K_i (45×)	N/A	Piret et al.[36]
N815S	affects a direct ACV-TP contact	r[b] (60–230×)	s	r[b] (3–4×)	N/A	N/A	Larder et al.,[28] Schubert et al.,[29] Larder and Darby,[37] and Furman et al.[39]
R842S	may change PNL loop DNA interactions	r (20×)	r (PAA)[a] (>10×)	hs (0.2×)	ACV-TP K_m (3.8×), k_{cat} (0.6×), Ki (2.5x)	increased	Huang et al.,[26] Gibbs et al.,[30] Chiou,[32] Coen et al.,[40] and Hall et al.[41]
F891C	would alter DNA primer positioning	r (6–35×)	r (4×)	hs (0.1×)	ACV-TP K_m (1.6×), k_{cat} (0.016×), K_i (6.2×)	N/A	Huang et al.[26] and Bestman-Smith and Boivin[42]
Y941H	would alter DNA primer positioning	r (9×)	r (11×)	N/A	ACV-TP K_m (5.8×), k_{cat} (0.27×), K_i (3.7×)	N/A	Huang et al.,[26] Bestman-Smith and Boivin,[42] Hwang et al.,[43] and Pelosi et al.[44]
N961K	would alter DNA primer positioning	r (5×)	s	s	ACV-TP K_m (3.3×), k_{cat} (0.26×), K_i (3.3×)	N/A	Huang et al.,[26] Gibbs et al.,[30] Chiou,[32] Bestman-Smith and Boivin,[42] and Coen et al.[45]

Effects of substitutions in the leftmost column on polymerase conformational dynamics, drug binding, or interactions with primer template based on the structures are noted in the second leftmost column. For W781V, E597K, A605V, and L774F substitutions, predicted effects are also based on molecular dynamic simulations reported in our study. The next four columns show viral phenotypes for drug susceptibility and replication fidelity demonstrated to be due to the mutation by marker rescue or transfer and sequencing.

r, resistant; ED_{50}, defined as ≥2-fold increase in the dose that decreases plaque formation by 50%; s, sensitive; hs, hypersensitive; defined as ≥1.3-fold decrease in ED_{50}. "×" denotes fold change in ED_{50} values. The second rightmost column shows effects apparent kinetic constants for ACV-TP incorporation and inhibition in steady-state assays. The rightmost column cites references for these viral phenotypes and apparent kinetic constants. This table's format is adapted from Piret and Boivin.[2]

[a]PAA, phosphonoacetic acid.

[b]By assaying drug susceptibilities from multiple independent isolates with the same mutation.

between the $L774_{Pol}$ side chain and surrounding residues are larger in the open conformation and smaller in the closed conformation (Figure S5H). The open conformation, but not the closed conformation, could possibly better accommodate the larger phenylalanine side chain (Figure S5I), thus explaining selective effects on structural fluctuations in the fingers domain in the closed conformation.

The RMSF calculations suggest that while resistance mutations may increase structural fluctuations in the fingers domain, nucleotide binding makes these structural fluctuations less pronounced

Please cite this article in press as: Shankar et al., Viral DNA polymerase structures reveal mechanisms of antiviral drug resistance, Cell (2024), https://doi.org/10.1016/j.cell.2024.07.048

(Figures 4G and 4H). This is likely because nucleotide binding stabilizes closure of the fingers. We next used structures of drug-bound complexes to perform simulations of WT HSV polymerase in the presence or absence of drugs. Simulations of the WT polymerase with and without ACV-TP show that, like with the presence of dTTP in the closed complex, the presence of ACV-TP decreases structural fluctuations of the fingers domain (Figures S6A and S6B). Conducting similar simulations with polymerase bound to foscarnet, a smaller ligand, also decreased structural fluctuations of the fingers domain (Figures S6C–S6E). When we compared *in silico* mutated polymerases to WT polymerases in the presence or absence of drugs, ACV-TP binding decreased structural fluctuations of both WT and W781V Pol (Figures S6F–S6I). This suggests that for this particular resistance mutant and drug combination, the defect caused by the more dynamic fingers that results in resistance would be observed during initial drug binding, but once the drug is bound (e.g., at high enough concentrations), the drug would still be incorporated. This finding is consistent with prior observations that at drug concentrations that are high enough, mutant enzymes can bind ACV-TP and catalyze its incorporation.[26] However, binding of foscarnet decreased structural fluctuations in the fingers domain of WT Pol more than it did in the W781V drug-resistant Pol (Figures S6J–S6M). These MD findings are consistent with a mechanism of drug resistance in which the more dynamic fingers of the W781V Pol mutant are less stabilized by the binding of foscarnet than are the fingers of the WT polymerase.

Therefore, MD analysis helps predict that certain resistance mutations increase structural fluctuations of the fingers domain in both the open and closed conformations (W781V, A605V, and E597K), while other mutations may selectively affect the closed conformation (L774F). The RMSF calculations suggest that while resistance mutations increase structural fluctuations in the fingers domain, ligand binding makes these structural fluctuations less pronounced by stabilizing closure of the fingers. We expect that the ternary complex is affected by drug-resistance mutations when the enzyme binds either the drug or natural substrates, but because the drugs make less or weaker contacts than do nucleotides to stabilize the closed conformation, drug binding is energetically disfavored over the binding of nucleotides. In support of this notion, the WT HSV Pol has a lower apparent K_m for nucleotide than for ACV-TP; moreover, mutants E597K and A605V have either a greater increase in apparent K_m or a greater decrease in apparent k_{cat} for ACV-TP than for nucleotide, respectively (Table 1).[26] The weaker contacts of ACV-TP to stabilize the closed conformation may explain the evidently greater effects on ACV-TP binding than on nucleotide by these substitutions. As foscarnet binding also favors the closed conformation, this may explain why these substitutions also confer resistance to pyrophosphate analogs. Importantly, increasing structural fluctuations of the fingers domain should not prevent normal nucleotides from stabilizing fingers domain closure, which they would do more readily than the weaker binding drugs, thereby permitting efficient catalysis.

Substitutions that would impact DNA template and primer interactions

Another class of distant substitutions that confer resistance to antivirals includes those likely to impact interactions the polymerase makes with the DNA primer or template. For example, Y941H, which was found in a clinical isolate, and F891C confer resistance to ACV and pyrophosphate analogs (Table 1).[42,43,46] The side chains of $Y941_{Pol}$ and $F891_{Pol}$ contact each other in the palm as a part of a cluster of mostly hydrophobic residues (Figure S2I). $Y941_{Pol}$ is in the "KK(K/R)Y" motif found in CRVII[43,47] and, together with $K953_{Pol}$ from CRV, helps align the primer 3′ end toward the active site by contacting the phosphate between the terminal residue and the previous residue in the translocated primer (Figures S2A, S2B, and S2I). The Y941H substitution would alter the contact with the phosphate, and the F891C substitution would likely increase the flexibility of the $Y941_{Pol}$ side chain and affect the strength and/or geometry of primer 3′ end positioning.

The N961K substitution in the Pol thumb within CRV confers ACV resistance but not foscarnet resistance (Table 1).[30,42,45] In the closed polymerase, N961K would alter contacts that $N961_{Pol}$ makes with the DNA backbone, and the longer lysine side chain would introduce a steric clash with the side chain of $R959_{Pol}$, a residue in CRV that interacts extensively with primer strand residues −4 and −5 (Figure 2C). The substitution would reduce the strength of primer binding and possibly distort the orientation of the primer end. Another substitution in this class, R842S, causes resistance to ACV and pyrophosphate analogs (Table 1).[30] R842S would remove key polar contacts $R842_{Pol}$ makes with $T839_{Pol}$, $Q697_{Pol}$, and $G698_{Pol}$ that tether the palm-NTD loop onto a helix in the palm and would affect the flexibility of the palm-NTD loop, which, as mentioned above, helps stabilize the dsDNA-to-ssDNA junction in the PT (Figures 2B and 2C). Thus, the R842S substitution would also likely destabilize binding and/or orientation of the template and primer.

R842S, F891C, Y941H, and N961K all cause increased apparent K_m and/or decreased apparent k_{cat} for both nucleotide and ACV-TP incorporation, but with greater effects observed with ACV-TP (Table 1).[26] The structures suggest that this effect is likely observed because ACV-TP provides weaker contacts than does a nucleotide to stabilize the ternary complex.

Structure of an editing polymerase complex

A subclass of particles seemed to adopt the editing conformation when we imaged the DNA-bound polymerase in the absence of nucleotide. Using a template containing a primer mismatch (PT3) (Figure S1B) that would distort the geometry of the DNA primer-template in the active site increased the number of particles in this subclass and allowed us to determine a structure of an editing holoenzyme to 3.3 Å resolution (Figures 5A, 5B, and S7A). The Pol fingers are, as expected, in an open conformation during editing (Figure 5A), but several differences can be observed when the structures of the closed, open, and the editing polymerases are compared. In the editing structure, the thumb maintains interactions with the DNA but rotates away from the Pol active site, pulling the primer end toward the Exo active site (Figure 5B). Additionally, contacts that the NTD side of the palm-NTD loop makes with the template ssDNA segment differ in the closed and editing polymerases (Figures 5C and 5D). The Exo β-hairpin transitions from providing contacts that mainly stabilize the ssDNA template in

Please cite this article in press as: Shankar et al., Viral DNA polymerase structures reveal mechanisms of antiviral drug resistance, Cell (2024), https://doi.org/10.1016/j.cell.2024.07.048

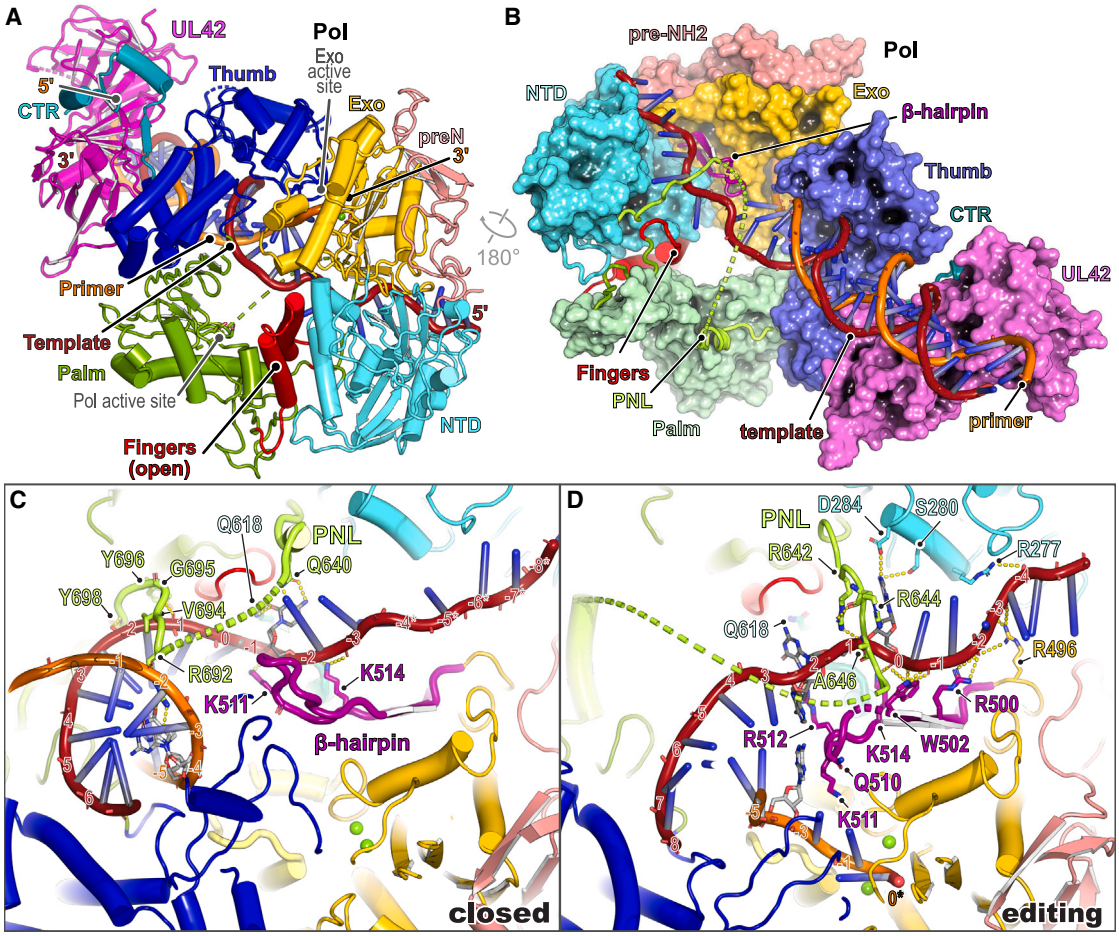

Figure 5. Structure of an editing HSV polymerase

(A) HSV polymerase bound to DNA primer template containing a mismatch at the primer 3′ end. The fingers are open, and the primer 3′ end is translocated into the Exo active site, which is 40 Å away from the Pol active site.

(B) Surface representation of the DNA-bound HSV polymerase in the editing conformation in a rotated view. The fingers, loops near the base of the fingers, palm-NTD loop (PNL), Exo β-hairpin motif, and DNA are shown as ribbon diagrams.

(C and D) Exo β-hairpin motif and palm-NTD loop interactions in the closed (C) and editing (D) polymerases. For the closed structure (C), the nucleotide residues that are labeled with asterisks were modeled but not deposited in structural coordinates due to weak density. For the editing structure (D), the nucleotide residue at the 3′ end of the primer (labeled with an asterisk) and one of the two Exo active site metals (see Figure S7B) were also modeled but not deposited in structural coordinates because of weak density.

See also Figure S7.

the closed conformation to providing contacts that stabilize the point of strand separation in the partially melted DNA duplex in the editing conformation (Figures 5C and 5D). We also docked the editing polymerase structure into the volume obtained from the subclass of particles that seemed to adopt the editing conformation when we imaged particles in the absence of nucleotide and with a PT that does not contain a mismatch (Video S2). This analysis confirmed that this subset of particles represents an editing polymerase.

Although maps for the editing polymerase complex had a global resolution of 3.3 Å, they were of poor quality where the ssDNA courses its way into the Exo active site, suggesting local flexibility (Figure S7A). Additionally, density was very weak for the terminal base at the 3′ end of the primer, and we observed strong density for only one of the two expected Exo active site metals. These features raise the possibility that the terminal primer base may have been excised by the Exo despite the presence of a phosphorothioate bond between the ultimate and penultimate bases in the primer (Figure S1B). We were nonetheless able to generate a model for the Exo active site based on discernible features for amino acid side chains and the expected geometry of the terminal base (Figure S7B). Two residues critical for Exo activity, $D368_{Pol}$ and $D581_{Pol}$, are positioned to interact with metal ions to allow for cleavage of the terminal base.[48–50] The Exo active site contacts with the 3′ primer end resemble those observed in the X-ray crystal structure of bacteriophage RB69 Pol (gp43) captured in the editing conformation (Figure S7C).[51]

Please cite this article in press as: Shankar et al., Viral DNA polymerase structures reveal mechanisms of antiviral drug resistance, Cell (2024), https://doi.org/10.1016/j.cell.2024.07.048

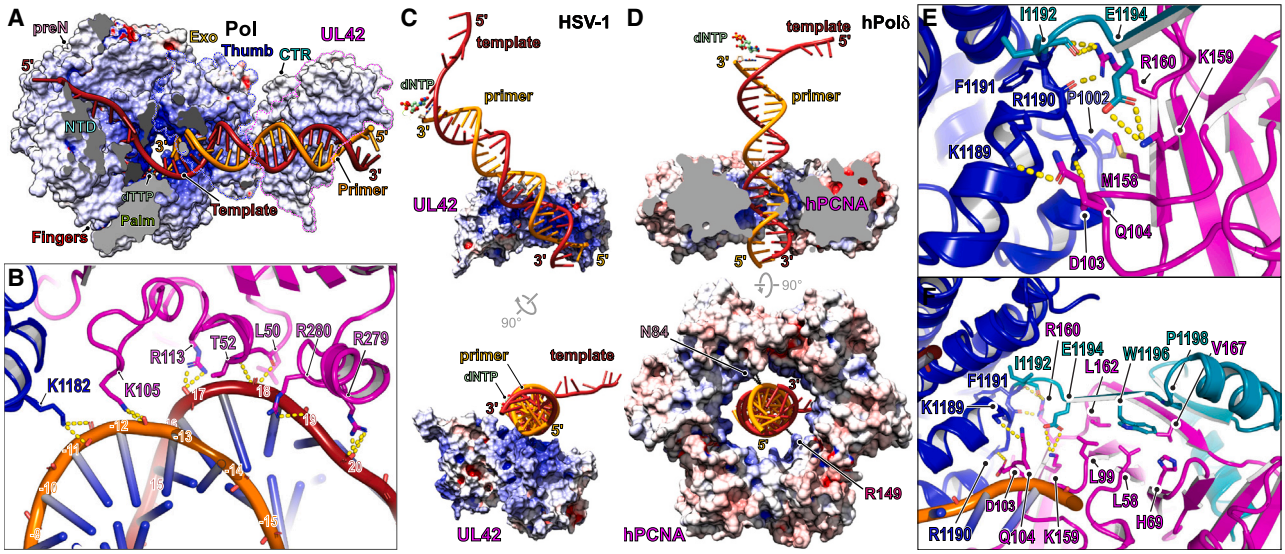

Figure 6. UL42 DNA binding and comparison to human PCNA

(A) Electrostatic surface potential of HSV polymerase bound to DNA in the closed conformation (bound to dTTP). DNA primer and template are shown as a ribbon diagram. The Pol thumb and UL42 surfaces are outlined.

(B) Closeup view of the UL42-DNA interface, highlighting Pol thumb and UL42 residues that contact DNA (<4 Å).

(C) Electrostatic surface potential representation of UL42 bound to DNA as part of the HSV polymerase. DNA is shown as a ribbon diagram, and bound nucleotide in the active site is shown as sticks. The catalytic subunit (Pol) is omitted for clarity. Top and bottom panels are different views.

(D) Electrostatic surface potential representation of the PCNA trimer surrounding DNA as part of human polymerase δ (PDB: 6TNY).[15] The DNA is shown as a ribbon diagram, and bound nucleotide in the active site is shown as sticks. Other subunits (e.g., catalytic and accessory subunits) are omitted for clarity. Top and bottom panels are different views. The positions of two PCNA residues (N84 and R149) that contact the DNA phosphate backbone (<4 Å) are indicated.

(E and F) Pol thumb (E) or Pol thumb and CTR (F) contacts with UL42. Contacts shown were not previously visualized in the structure of UL42 bound to Pol CTR residues 1,200–1,235.[5]

A drug-resistant mutant adopts the editing conformation

We next turned again to single-particle cryo-EM analysis to test the prediction that certain HSV Pol mutations associated with ACV and foscarnet resistance that are remote from the Pol active site influence holoenzyme conformational dynamics. We chose W781V in the fingers domain, which is at the interface with the NTD in both the open and closed conformations (Figures 4E and 4F). Our MD simulations suggested that the W781V mutation would increase structural fluctuations in the fingers domain in both of these conformations (Figures 4B–4D).

We expressed HSV Pol containing the W781V mutation and confirmed that the protein was active in a DNA elongation assay (Figure S7D). We determined the cryo-EM structure of the mutant polymerase (W781V Pol and UL42) bound to PT1 without nucleotide (Figures S1B and S7E). Remarkably, we did not observe any volumes during 3D classification to suggest the presence of open/closed holoenzyme conformations, and 3D classification of particles resulted in a single map (5.1 Å resolution) that could only fit the editing polymerase structure (Figure S7F; Video S3). Importantly, as in the WT editing complex, the fingers remain open and the thumb rotates toward the Exo domain in the mutant polymerase complex (Figure S7F). Therefore, a single residue mutation in a >1,200 amino acid polymerase catalytic subunit allowed it to favor the editing conformation when samples were imaged in the absence of nucleotide. This finding is strikingly similar to how WT RB69 gp43, a Pol that is not susceptible to foscarnet and poorly incorporates ACV-TP,[52] adopts the editing conformation when crystallized with mismatch-free DNA primer-template in the absence of a nucleotide.[51]

Mode of interaction of UL42 with DNA

UL42 extends a positively charged surface that would otherwise end with the Pol thumb (Figure 6A). This extension corresponds roughly to a complete turn of a dsDNA helix, consistent with the results of footprinting experiments.[10,53] UL42 interactions with DNA are overall similar in the closed, open, and editing conformations, and UL42 moves as a rigid module with Pol in concert during its conformational transitions. As predicted from the original UL42 structure and supported by mutational analysis and cross-linking data,[5,12,54] a cluster of UL42 basic residues binds the backbone of newly synthesized DNA (Figure 6B). These contacts include several arginines that are conserved among α-herpesviruses for which substitutions have been shown to reduce UL42 binding to DNA, processive DNA synthesis, replication fidelity, and viral replication (e.g., $R113_{UL42}$, $R279_{UL42}$, and $R280_{UL42}$) (Figure 6B).[12,54,55] Comparison of the trajectories of DNA bound to the HSV polymerase holoenzyme with the human DNA polymerase δ/PCNA complex[15] reveals marked differences in the angle with which DNA traverses the back face of the respective processivity factors (Figures 6C and 6D). Additionally, UL42 makes much closer contacts per monomer with DNA than does PCNA; the UL42 monomer makes multiple direct contacts

Please cite this article in press as: Shankar et al., Viral DNA polymerase structures reveal mechanisms of antiviral drug resistance, Cell (2024), https://doi.org/10.1016/j.cell.2024.07.048

(<4 Å) with the DNA phosphate backbone, while the trimeric PCNA rings in polymerase δ make few contacts (Figures 6B–6D).[15,16]

As in the X-ray crystal structure of UL42 bound to an HSV Pol C-terminal fragment,[5] Pol's interaction with UL42 involves an α-β-α motif, whose C-terminal α-helix makes most of the UL42 contacts (Figure 1B). We also observed additional interactions that two thumb helices and associated loops and the CTR make with UL42 (Figures 6E and 6F). The interactions involve $K1189_{Pol}$, $R1190_{Pol}$, $I1192_{Pol}$, and $E1194_{Pol}$. CTR-UL42 interactions also include an additional small β-strand and prominent polar and hydrophobic contacts made by $W1196_{Pol}$. Deletion of these CTR residues does not eliminate the interaction with UL42 but does weaken it.[56] The newly visualized Pol-UL42 contacts may regulate the angle between the polymerase and processivity factor to maximize protein-DNA charge-charge interactions.

DISCUSSION

Our structural analysis suggests that HSV polymerase frequently samples the closed conformation in the absence of a substrate in the active site and that mutations that increase structural fluctuations in the fingers domain result in drug resistance by disfavoring the binding of drugs that make weaker and/or fewer contacts than would incoming nucleotides. Our findings suggest that conformational dynamics are critical for polymerase resistance to ACV and foscarnet, and they may be relevant to resistance and thus selectivity involving other drug-target combinations.[57,58] A large body of literature directly links conformational dynamics and the activity and fidelity of viral RNA-dependent RNA polymerases.[59–63] This important work, which has mostly used picornavirus polymerases as model systems, has demonstrated mechanisms of allosteric control on enzyme substrate selectivity through effects on the dynamics of conserved structural motifs. Our work on HSV polymerase suggests that these fundamental mechanisms extend beyond the polymerases of RNA viruses and apply to the polymerases of some DNA viruses as well.

Drug-resistant polymerases having fingers domains that are more dynamic may translate into a better ability to discriminate proper nucleotide incorporation, as engagement of the incorrect nucleotide opposite the templating base would provide less binding energy to stabilize the closed state. This notion is supported by studies of the L774F HSV Pol mutant, which has an antimutator phenotype in addition to ACV and foscarnet resistance,[35,38] and which our MD analysis suggests would have more dynamic fingers in the closed conformation.

The observation that the W781V polymerase holoenzyme in the absence of substrate in the active site adopted the editing conformation raises the possibility that this mutant may have elevated Exo activity. Although we did not test this directly, a more frequent transition of the primer end to the Exo active site could provide an attractive mechanism for the antimutator phenotype observed for some drug-resistant polymerases that have more dynamic fingers. Additionally, at least two of the four mutations that our structural and MD simulations predict would increase structural fluctuations in the fingers domain and/or may favor opening of the fingers (A605V and L774F) evidently confer hypersensitivity to aphidicolin, a molecule that is known to bind the open conformation of at least one family B polymerase (human DNA polymerase α) (Table 1).[64] Hypersensitivity to aphidicolin is also consistent with our hypothesized mechanism of drug resistance for ACV and foscarnet.

One could speculate that by having a higher propensity to adopt the closed conformation, herpesvirus polymerases, which function as part of much simpler replisomes,[65] may more rapidly incorporate nucleotides without factors used by the eukaryotic replication machinery for rapid fork movement.[6,66–68] More rapid incorporation of nucleotides could be acting in concert with other mechanisms to favor HSV replication in infected cells, including virus-encoded enzymes such as ribonucleotide reductase and thymidine kinase that increase nucleotide pools.

Although no structures of a herpesvirus Pol bound to ACV or foscarnet had previously been reported, an X-ray crystal structure of foscarnet and DNA primer-template bound to a bacteriophage RB69 gp43 mutant that contains nine substitutions in the fingers domain derived from human cytomegalovirus Pol sequence is available.[69] Unlike crystal structures of WT RB69 Pol, which crystallized in the editing conformation without nucleotide,[51] the mutant RB69 Pol crystallized in the closed, untranslocated state even in the absence of foscarnet or nucleotide in the active site. The structures suggested that a particular fingers domain mutation present in the mutant RB69 Pol, V478W (which is at the position equivalent to HSV $W781_{Pol}$), biased the enzyme toward the closed conformation.[69] Unlike the HSV Pol W781V drug-resistance mutation we studied here, the V478W mutation in RB69 Pol replaces a naturally occurring valine with a tryptophan. The V478W substitution, by biasing the RB69 enzyme toward the closed conformation, would be expected to have the inverse effect of the W781V drug-resistant variant, and it indeed renders the mutant RB69 Pol susceptible to foscarnet inhibition.[69] Although a structure of DNA-bound herpesvirus polymerase in the open or closed conformations was not available, the elegant structural and mutational studies of the engineered RB69 gp43 allowed the authors to propose that herpesvirus Pols may be intrinsically biased toward the closed state, thus influencing drug selectivity.[36,69] This hypothesis is also supported by our cryo-EM analysis of nucleotide-free HSV polymerase.

When the HSV polymerase holoenzyme and the RB69 Pol structures are compared, in the closed, foscarnet-bound HSV polymerase structure reported here, HSV $R789_{Pol}$ contacts foscarnet while the equivalent residue in RB69 gp43, K486, does not contact the drug (Figures 3D and S3E). Additionally, metal ions A and B were present in the mutant RB69 gp43-foscarnet complex structure rather than ions B and C in the HSV Pol structure, suggesting that the HSV polymerase foscarnet-bound structure may be more consistent with a post-incorporation intermediate.

We found that HSV Pol's dynamic equilibrium includes not only the closed and open conformations but also the editing conformation. Analyses of pre-steady-state experiments have suggested that the rate-limiting step in polymerase activity (~150 s^{-1}) is closing of the fingers,[66] which is relatively fast, while, based on measurements of extension of mismatched primers, it has been reported that movement of the primer between the Pol and Exo active sites is relatively inefficient.[70] Interestingly, several groups have studied whether pyrophosphate

analogs inhibit Exo activity, and most found that they do.[71–75] As foscarnet favors a closed, untranslocated state, we suggest that the fingers needing to open during editing explains that finding; specifically, that foscarnet binding would impair movement of the primer to the Exo domain of the same polymerase holoenzyme.

We show that positioning of UL42 maximizes charge-charge interactions extending from the thumb through the processivity factor (Figures 6A and 6B). Such an extensive charge-charge interaction surface would facilitate processive DNA synthesis and likely allow UL42 to slide on DNA as part of the assembled holoenzyme, which would be faster movement than the hopping observed when UL42 alone interacts with DNA in solution.[11,76,77] The structures help clarify mechanisms of processive DNA synthesis by herpesvirus polymerases and could serve as templates to aid in the design of allosteric inhibitors that trap Pol conformational states and thus help combat emerging resistance to antivirals. They also suggest that determining cryo-EM structures of additional viral or eukaryotic B-family DNA polymerases in the absence of nucleotides could provide important comparative information on the dynamics of their nucleotide-free states.

Limitations of the study

Conformational dynamics might be affected by interactions of HSV polymerase with other proteins. Additional structures and MD simulations could help further delineate antiviral drug-resistance mechanisms. Future experiments to assess the effects of drug-resistance mutations on HSV polymerase fingers domain conformational dynamics could be performed using single-molecule fluorescence resonance energy transfer.[78] ACV, in addition to being a competitive inhibitor of nucleotide binding, is an obligate chain terminator, and its incorporation into growing DNA results in a "dead-end" complex in which the next nucleotide is bound. Determining the cryo-EM structure of this dead-end complex in which the DNA primer is terminated by ACV may also be important for understanding mechanisms of drug action and resistance.

STAR★METHODS

Detailed methods are provided in the online version of this paper and include the following:

- KEY RESOURCES TABLE
- RESOURCE AVAILABILITY
  - Lead contact
  - Materials availability
  - Data and code availability
- EXPERIMENTAL MODEL AND STUDY PARTICIPANT DETAILS
  - Insect cells
  - Bacterial cells
- METHOD DETAILS
  - Protein expression and purification
  - DNA elongation assays
  - Cryo-EM sample preparation
  - Cryo-EM data collection
  - Cryo-EM image processing
  - Model building and refinement
  - 3D variability analysis
  - *In silico* modeling and MD simulations
- QUANTIFICATION AND STASTICAL ANALYSIS

SUPPLEMENTAL INFORMATION

Supplemental information can be found online at https://doi.org/10.1016/j.cell.2024.07.048.

ACKNOWLEDGMENTS

Cryo-EM data were collected at the Harvard Cryo-EM Center for Structural Biology at Harvard Medical School. We would like to thank Jessica Lawler for providing the HSV Pol protein used in the initial structure determination experiments. This work was supported by an NIH award R21 AI141940 to D.M.C. and J.A. and NIH award R01 AI19838 to D.M.C. and J.M.H. This work was also supported by a Centers for Integrated Solutions in Infectious Diseases (CISID) grant to J.A. J.P. is a Chutian Scholar.

AUTHOR CONTRIBUTIONS

Conceptualization: S.S., J.P., P.Y., Y.B., M.S., D.M.C., and J.A.; investigation: S.S., J.P., P.Y., Y.B, G.O., Z.Y., P.M., D.J.F., J.M.H., M.S., D.M.C., and J.A.; writing – original draft: S.S., J.P., Y.B., D.M.C., and J.A.; writing – review and editing: S.S., J.P., P.Y., Y.B., G.O., P.M., D.J.F., J.M.H., M.S., D.M.C., and J.A.; funding acquisition, J.M.H., D.M.C., and J.A.

DECLARATION OF INTERESTS

The authors declare no competing interests.

Received: December 22, 2022
Revised: January 27, 2024
Accepted: July 26, 2024
Published: August 27, 2024

REFERENCES

1. Coen, D.M., Namchuk, M.N., and Kuritzkes, D.R. (2023). Antiviral agents. In Fields Virology, P.M. Howley, D.M. Knipe, S.M. Whelan, J.I. Cohen, B. Damania, and E.O. Freed, eds. (Wolters Kluwer), pp. 353–397.
2. Piret, J., and Boivin, G. (2021). DNA polymerases of herpesviruses and their inhibitors. Enzymes *50*, 79–132. https://doi.org/10.1016/bs.enz.2021.07.003.
3. Gottlieb, J., Marcy, A.I., Coen, D.M., and Challberg, M.D. (1990). The herpes simplex virus type 1 UL42 gene product: a subunit of DNA polymerase that functions to increase processivity. J. Virol. *64*, 5976–5987. https://doi.org/10.1128/JVI.64.12.5976-5987.1990.
4. Liu, S., Knafels, J.D., Chang, J.S., Waszak, G.A., Baldwin, E.T., Deibel, M.R., Jr., Thomsen, D.R., Homa, F.L., Wells, P.A., Tory, M.C., et al. (2006). Crystal structure of the herpes simplex virus 1 DNA polymerase. J. Biol. Chem. *281*, 18193–18200. https://doi.org/10.1074/jbc.M602414200.
5. Zuccola, H.J., Filman, D.J., Coen, D.M., and Hogle, J.M. (2000). The crystal structure of an unusual processivity factor, herpes simplex virus UL42, bound to the C terminus of its cognate polymerase. Mol. Cell *5*, 267–278. https://doi.org/10.1016/s1097-2765(00)80422-0.
6. Weisshart, K., Chow, C.S., and Coen, D.M. (1999). Herpes simplex virus processivity factor UL42 imparts increased DNA-binding specificity to the viral DNA polymerase and decreased dissociation from primer-template without reducing the elongation rate. J. Virol. *73*, 55–66. https://doi.org/10.1128/JVI.73.1.55-66.1999.
7. Randell, J.C.W., and Coen, D.M. (2004). The herpes simplex virus processivity factor, UL42, binds DNA as a monomer. J. Mol. Biol. *335*, 409–413. https://doi.org/10.1016/j.jmb.2003.10.064.
8. Vaughan, P.J., Purifoy, D.J., and Powell, K.L. (1985). DNA-binding protein associated with herpes simplex virus DNA polymerase. J. Virol. *53*, 501–508. https://doi.org/10.1128/JVI.53.2.501-508.1985.

9. Gallo, M.L., Jackwood, D.H., Murphy, M., Marsden, H.S., and Parris, D.S. (1988). Purification of the herpes simplex virus type 1 65-kilodalton DNA-binding protein: properties of the protein and evidence of its association with the virus-encoded DNA polymerase. J. Virol. *62*, 2874–2883. https://doi.org/10.1128/JVI.62.8.2874-2883.1988.

10. Gottlieb, J., and Challberg, M.D. (1994). Interaction of herpes simplex virus type 1 DNA polymerase and the UL42 accessory protein with a model primer template. J. Virol. *68*, 4937–4945. https://doi.org/10.1128/JVI.68.8.4937-4945.1994.

11. Komazin-Meredith, G., Mirchev, R., Golan, D.E., van Oijen, A.M., and Coen, D.M. (2008). Hopping of a processivity factor on DNA revealed by single-molecule assays of diffusion. Proc. Natl. Acad. Sci. USA *105*, 10721–10726. https://doi.org/10.1073/pnas.0802676105.

12. Komazin-Meredith, G., Santos, W.L., Filman, D.J., Hogle, J.M., Verdine, G.L., and Coen, D.M. (2008). The positively charged surface of herpes simplex virus UL42 mediates DNA binding. J. Biol. Chem. *283*, 6154–6161. https://doi.org/10.1074/jbc.M708691200.

13. Hayes, R.P., Heo, M.R., Mason, M., Reid, J., Burlein, C., Armacost, K.A., Tellers, D.M., Raheem, I., Shaw, A.W., Murray, E., et al. (2021). Structural understanding of non-nucleoside inhibition in an elongating herpesvirus polymerase. Nat. Commun. *12*, 3040. https://doi.org/10.1038/s41467-021-23312-8.

14. Zhang, J., Chung, D.W., Tan, C.K., Downey, K.M., Davie, E.W., and So, A.G. (1991). Primary structure of the catalytic subunit of calf thymus DNA polymerase delta: sequence similarities with other DNA polymerases. Biochemistry *30*, 11742–11750. https://doi.org/10.1021/bi00115a002.

15. Lancey, C., Tehseen, M., Raducanu, V.S., Rashid, F., Merino, N., Ragan, T.J., Savva, C.G., Zaher, M.S., Shirbini, A., Blanco, F.J., et al. (2020). Structure of the processive human Pol delta holoenzyme. Nat. Commun. *11*, 1109. https://doi.org/10.1038/s41467-020-14898-6.

16. Zheng, F., Georgescu, R.E., Li, H., and O'Donnell, M.E. (2020). Structure of eukaryotic DNA polymerase delta bound to the PCNA clamp while encircling DNA. Proc. Natl. Acad. Sci. USA *117*, 30344–30353. https://doi.org/10.1073/pnas.2017637117.

17. Doublié, S., and Zahn, K.E. (2014). Structural insights into eukaryotic DNA replication. Front. Microbiol. *5*, 444. https://doi.org/10.3389/fmicb.2014.00444.

18. Robert, X., and Gouet, P. (2014). Deciphering key features in protein structures with the new ENDscript server. Nucleic Acids Res. *42*, W320–W324. https://doi.org/10.1093/nar/gku316.

19. Franklin, M.C., Wang, J., and Steitz, T.A. (2001). Structure of the replicating complex of a pol alpha family DNA polymerase. Cell *105*, 657–667. https://doi.org/10.1016/s0092-8674(01)00367-1.

20. Hogg, M., Osterman, P., Bylund, G.O., Ganai, R.A., Lundström, E.B., Sauer-Eriksson, A.E., and Johansson, E. (2014). Structural basis for processive DNA synthesis by yeast DNA polymerase epsilon. Nat. Struct. Mol. Biol. *21*, 49–55. https://doi.org/10.1038/nsmb.2712.

21. Baranovskiy, A.G., Duong, V.N., Babayeva, N.D., Zhang, Y., Pavlov, Y.I., Anderson, K.S., and Tahirov, T.H. (2018). Activity and fidelity of human DNA polymerase alpha depend on primer structure. J. Biol. Chem. *293*, 6824–6843. https://doi.org/10.1074/jbc.RA117.001074.

22. Punjani, A., and Fleet, D.J. (2021). 3D variability analysis: Resolving continuous flexibility and discrete heterogeneity from single particle cryo-EM. J. Struct. Biol. *213*, 107702. https://doi.org/10.1016/j.jsb.2021.107702.

23. Weisshart, K., Kuo, A.A., Painter, G.R., Wright, L.L., Furman, P.A., and Coen, D.M. (1993). Conformational changes induced in herpes simplex virus DNA polymerase upon DNA binding. Proc. Natl. Acad. Sci. USA *90*, 1028–1032. https://doi.org/10.1073/pnas.90.3.1028.

24. Elion, G.B., Furman, P.A., Fyfe, J.A., de Miranda, P., Beauchamp, L., and Schaeffer, H.J. (1977). Selectivity of action of an antiherpetic agent, 9-(2-hydroxyethoxymethyl) guanine. Proc. Natl. Acad. Sci. USA *74*, 5716–5720. https://doi.org/10.1073/pnas.74.12.5716.

25. Reardon, J.E., and Spector, T. (1989). Herpes simplex virus type 1 DNA polymerase. Mechanism of inhibition by acyclovir triphosphate. J. Biol. Chem. *264*, 7405–7411. https://doi.org/10.1016/S0021-9258(18)83248-3.

26. Huang, L., Ishii, K.K., Zuccola, H., Gehring, A.M., Hwang, C.B., Hogle, J., and Coen, D.M. (1999). The enzymological basis for resistance of herpesvirus DNA polymerase mutants to acyclovir: relationship to the structure of alpha-like DNA polymerases. Proc. Natl. Acad. Sci. USA *96*, 447–452. https://doi.org/10.1073/pnas.96.2.447.

27. Reno, J.M., Lee, L.F., and Boezi, J.A. (1978). Inhibition of herpesvirus replication and herpesvirus-induced deoxyribonucleic acid polymerase by phosphonoformate. Antimicrob. Agents Chemother. *13*, 188–192. https://doi.org/10.1128/AAC.13.2.188.

28. Larder, B.A., Kemp, S.D., and Darby, G. (1987). Related functional domains in virus DNA polymerases. EMBO J. *6*, 169–175. https://doi.org/10.1002/j.1460-2075.1987.tb04735.x.

29. Schubert, A., Gentner, E., Bohn, K., Schwarz, M., Mertens, T., and Sauerbrei, A. (2014). Single nucleotide polymorphisms of thymidine kinase and DNA polymerase genes in clinical herpes simplex virus type 1 isolates associated with different resistance phenotypes. Antiviral Res. *107*, 16–22. https://doi.org/10.1016/j.antiviral.2014.03.015.

30. Gibbs, J.S., Chiou, H.C., Bastow, K.F., Cheng, Y.C., and Coen, D.M. (1988). Identification of amino acids in herpes simplex virus DNA polymerase involved in substrate and drug recognition. Proc. Natl. Acad. Sci. USA *85*, 6672–6676. https://doi.org/10.1073/pnas.85.18.6672.

31. Coen, D.M., Aschman, D.P., Gelep, P.T., Retondo, M.J., Weller, S.K., and Schaffer, P.A. (1984). Fine mapping and molecular cloning of mutations in the herpes simplex virus DNA polymerase locus. J. Virol. *49*, 236–247. https://doi.org/10.1128/JVI.49.1.236-247.1984.

32. Chiou, H.C. (1988). A combined pharmacological and genetic analysis of the herpes simplex virus DNA polymerase. PhD Thesis (Harvard University).

33. Saijo, M., Suzutani, T., Morikawa, S., and Kurane, I. (2005). Genotypic characterization of the DNA polymerase and sensitivity to antiviral compounds of foscarnet-resistant herpes simplex virus type 1 (HSV-1) derived from a foscarnet-sensitive HSV-1 strain. Antimicrob. Agents Chemother. *49*, 606–611. https://doi.org/10.1128/AAC.49.2.606-611.2005.

34. Bastow, K.F., Derse, D.D., and Cheng, Y.C. (1983). Susceptibility of phosphonoformic acid-resistant herpes simplex virus variants to arabinosylnucleosides and aphidicolin. Antimicrob. Agents Chemother. *23*, 914–917. https://doi.org/10.1128/AAC.23.6.914.

35. Hwang, Y.T., Zuccola, H.J., Lu, Q., and Hwang, C.B.C. (2004). A point mutation within conserved region VI of herpes simplex virus type 1 DNA polymerase confers altered drug sensitivity and enhances replication fidelity. J. Virol. *78*, 650–657. https://doi.org/10.1128/jvi.78.2.650-657.2004.

36. Piret, J., Goyette, N., Eckenroth, B.E., Drouot, E., Götte, M., and Boivin, G. (2015). Contrasting effects of W781V and W780V mutations in helix N of herpes simplex virus 1 and human cytomegalovirus DNA polymerases on antiviral drug susceptibility. J. Virol. *89*, 4636–4644. https://doi.org/10.1128/JVI.03360-14.

37. Larder, B.A., and Darby, G. (1986). Susceptibility to other antiherpes drugs of pathogenic variants of herpes simplex virus selected for resistance to acyclovir. Antimicrob. Agents Chemother. *29*, 894–898. https://doi.org/10.1128/AAC.29.5.894.

38. Tian, W., Hwang, Y.T., Lu, Q., and Hwang, C.B.C. (2009). Finger domain mutation affects enzyme activity, DNA replication efficiency, and fidelity of an exonuclease-deficient DNA polymerase of herpes simplex virus type 1. J. Virol. *83*, 7194–7201. https://doi.org/10.1128/JVI.00632-09.

39. Furman, P.A., Coen, D.M., St Clair, M.H., and Schaffer, P.A. (1981). Acyclovir-resistant mutants of herpes simplex virus type 1 express altered DNA polymerase or reduced acyclovir phosphorylating activities. J. Virol. *40*, 936–941. https://doi.org/10.1128/JVI.40.3.936-941.1981.

40. Coen, D.M., Furman, P.A., Aschman, D.P., and Schaffer, P.A. (1983). Mutations in the herpes simplex virus DNA polymerase gene conferring

hypersensitivity to aphidicolin. Nucleic Acids Res. *11*, 5287–5297. https://doi.org/10.1093/nar/11.15.5287.

41. Hall, J.D., Coen, D.M., Fisher, B.L., Weisslitz, M., Randall, S., Almy, R.E., Gelep, P.T., and Schaffer, P.A. (1984). Generation of genetic diversity in herpes simplex virus: an antimutator phenotype maps to the DNA polymerase locus. Virology *132*, 26–37. https://doi.org/10.1016/0042-6822(84)90088-6.
42. Bestman-Smith, J., and Boivin, G. (2003). Drug resistance patterns of recombinant herpes simplex virus DNA polymerase mutants generated with a set of overlapping cosmids and plasmids. J. Virol. *77*, 7820–7829. https://doi.org/10.1128/jvi.77.14.7820-7829.2003.
43. Hwang, C.B., Ruffner, K.L., and Coen, D.M. (1992). A point mutation within a distinct conserved region of the herpes simplex virus DNA polymerase gene confers drug resistance. J. Virol. *66*, 1774–1776. https://doi.org/10.1128/JVI.66.3.1774-1776.1992.
44. Pelosi, E., Hicks, K.A., Sacks, S.L., and Coen, D.M. (1992). Heterogeneity of a herpes simplex virus clinical isolate exhibiting resistance to acyclovir and foscarnet. Adv. Exp. Med. Biol. *312*, 151–158. https://doi.org/10.1007/978-1-4615-3462-4_15.
45. Coen, D.M., Fleming, H.E., Jr., Leslie, L.K., and Retondo, M.J. (1985). Sensitivity of arabinosyladenine-resistant mutants of herpes simplex virus to other antiviral drugs and mapping of drug hypersensitivity mutations to the DNA polymerase locus. J. Virol. *53*, 477–488. https://doi.org/10.1128/JVI.53.2.477-488.1985.
46. Marcy, A.I., Hwang, C.B., Ruffner, K.L., and Coen, D.M. (1990). Engineered herpes simplex virus DNA polymerase point mutants: the most highly conserved region shared among alpha-like DNA polymerases is involved in substrate recognition. J. Virol. *64*, 5883–5890. https://doi.org/10.1128/JVI.64.12.5883-5890.1990.
47. Braithwaite, D.K., and Ito, J. (1993). Compilation, alignment, and phylogenetic relationships of DNA polymerases. Nucleic Acids Res. *21*, 787–802. https://doi.org/10.1093/nar/21.4.787.
48. Hwang, Y.T., Smith, J.F., Gao, L., and Hwang, C.B. (1998). Mutations in the Exo III motif of the herpes simplex virus DNA polymerase gene can confer altered drug sensitivities. Virology *246*, 298–305. https://doi.org/10.1006/viro.1998.9201.
49. Hwang, Y.T., Liu, B.Y., Coen, D.M., and Hwang, C.B. (1997). Effects of mutations in the Exo III motif of the herpes simplex virus DNA polymerase gene on enzyme activities, viral replication, and replication fidelity. J. Virol. *71*, 7791–7798. https://doi.org/10.1128/JVI.71.10.7791-7798.1997.
50. Hall, J.D., Orth, K.L., Sander, K.L., Swihart, B.M., and Senese, R.A. (1995). Mutations within conserved motifs in the 3'-5' exonuclease domain of herpes simplex virus DNA polymerase. J. Gen. Virol. *76*, 2999–3008. https://doi.org/10.1099/0022-1317-76-12-2999.
51. Shamoo, Y., and Steitz, T.A. (1999). Building a replisome from interacting pieces: sliding clamp complexed to a peptide from DNA polymerase and a polymerase editing complex. Cell *99*, 155–166. https://doi.org/10.1016/s0092-8674(00)81647-5.
52. Tchesnokov, E.P., Obikhod, A., Schinazi, R.F., and Götte, M. (2009). Engineering of a chimeric RB69 DNA polymerase sensitive to drugs targeting the cytomegalovirus enzyme. J. Biol. Chem. *284*, 26439–26446. https://doi.org/10.1074/jbc.M109.012500.
53. Randell, J.C., and Coen, D.M. (2001). Linear diffusion on DNA despite high-affinity binding by a DNA polymerase processivity factor. Mol. Cell *8*, 911–920. https://doi.org/10.1016/s1097-2765(01)00355-0.
54. Randell, J.C.W., Komazin, G., Jiang, C., Hwang, C.B.C., and Coen, D.M. (2005). Effects of substitutions of arginine residues on the basic surface of herpes simplex virus UL42 support a role for DNA binding in processive DNA synthesis. J. Virol. *79*, 12025–12034. https://doi.org/10.1128/JVI.79.18.12025-12034.2005.
55. Jiang, C., Hwang, Y.T., Wang, G., Randell, J.C.W., Coen, D.M., and Hwang, C.B.C. (2007). Herpes simplex virus mutants with multiple substitutions affecting DNA binding of UL42 are impaired for viral replication and DNA synthesis. J. Virol. *81*, 12077–12079. https://doi.org/10.1128/JVI.01133-07.
56. Digard, P., Bebrin, W.R., Weisshart, K., and Coen, D.M. (1993). The extreme C terminus of herpes simplex virus DNA polymerase is crucial for functional interaction with processivity factor UL42 and for viral replication. J. Virol. *67*, 398–406. https://doi.org/10.1128/JVI.67.1.398-406.1993.
57. Leidner, F., Kurt Yilmaz, N., and Schiffer, C.A. (2021). Deciphering complex mechanisms of resistance and loss of potency through coupled molecular dynamics and machine learning. J. Chem. Theory Comput. *17*, 2054–2064. https://doi.org/10.1021/acs.jctc.0c01244.
58. Henes, M., Lockbaum, G.J., Kosovrasti, K., Leidner, F., Nachum, G.S., Nalivaika, E.A., Lee, S.K., Spielvogel, E., Zhou, S., Swanstrom, R., et al. (2019). Picomolar to micromolar: elucidating the role of distal mutations in HIV-1 protease in conferring drug resistance. ACS Chem. Biol. *14*, 2441–2452. https://doi.org/10.1021/acschembio.9b00370.
59. Moustafa, I.M., Shen, H., Morton, B., Colina, C.M., and Cameron, C.E. (2011). Molecular dynamics simulations of viral RNA polymerases link conserved and correlated motions of functional elements to fidelity. J. Mol. Biol. *410*, 159–181. https://doi.org/10.1016/j.jmb.2011.04.078.
60. Moustafa, I.M., Korboukh, V.K., Arnold, J.J., Smidansky, E.D., Marcotte, L.L., Gohara, D.W., Yang, X., Sánchez-Farrán, M.A., Filman, D., Maranas, J.K., et al. (2014). Structural dynamics as a contributor to error-prone replication by an RNA-dependent RNA polymerase. J. Biol. Chem. *289*, 36229–36248. https://doi.org/10.1074/jbc.M114.616193.
61. Shi, J., Perryman, J.M., Yang, X., Liu, X., Musser, D.M., Boehr, A.K., Moustafa, I.M., Arnold, J.J., Cameron, C.E., and Boehr, D.D. (2019). Rational control of poliovirus RNA-dependent RNA polymerase fidelity by modulating motif-D loop conformational dynamics. Biochemistry *58*, 3735–3743. https://doi.org/10.1021/acs.biochem.9b00497.
62. Winston, D.S., and Boehr, D.D. (2021). Allosteric and dynamic control of RNA-dependent RNA polymerase function and fidelity. Enzymes *49*, 149–193. https://doi.org/10.1016/bs.enz.2021.06.001.
63. Pfeiffer, J.K., and Kirkegaard, K. (2003). A single mutation in poliovirus RNA-dependent RNA polymerase confers resistance to mutagenic nucleotide analogs via increased fidelity. Proc. Natl. Acad. Sci. USA *100*, 7289–7294. https://doi.org/10.1073/pnas.1232294100.
64. Baranovskiy, A.G., Babayeva, N.D., Suwa, Y., Gu, J., Pavlov, Y.I., and Tahirov, T.H. (2014). Structural basis for inhibition of DNA replication by aphidicolin. Nucleic Acids Res. *42*, 14013–14021. https://doi.org/10.1093/nar/gku1209.
65. Weller, S.K., and Coen, D.M. (2012). Herpes simplex viruses: mechanisms of DNA replication. Cold Spring Harb. Perspect. Biol. *4*, a013011. https://doi.org/10.1101/cshperspect.a013011.
66. Chaudhuri, M., Song, L., and Parris, D.S. (2003). The herpes simplex virus type 1 DNA polymerase processivity factor increases fidelity without altering pre-steady-state rate constants for polymerization or excision. J. Biol. Chem. *278*, 8996–9004. https://doi.org/10.1074/jbc.M210023200.
67. Dieckman, L.M., Johnson, R.E., Prakash, S., and Washington, M.T. (2010). Pre-steady state kinetic studies of the fidelity of nucleotide incorporation by yeast DNA polymerase delta. Biochemistry *49*, 7344–7350. https://doi.org/10.1021/bi100556m.
68. Yeeles, J.T.P., Janska, A., Early, A., and Diffley, J.F.X. (2017). How the eukaryotic replisome achieves rapid and efficient DNA replication. Mol. Cell *65*, 105–116. https://doi.org/10.1016/j.molcel.2016.11.017.
69. Zahn, K.E., Tchesnokov, E.P., Götte, M., and Doublié, S. (2011). Phosphonoformic acid inhibits viral replication by trapping the closed form of the DNA polymerase. J. Biol. Chem. *286*, 25246–25255. https://doi.org/10.1074/jbc.M111.248864.
70. Vashishtha, A.K., and Kuchta, R.D. (2015). Polymerase and exonuclease activities in herpes simplex virus type 1 DNA polymerase are not highly coordinated. Biochemistry *54*, 240–249. https://doi.org/10.1021/bi500840v.

71. Derse, D., and Cheng, Y.C. (1981). Herpes simplex virus type I DNA polymerase. Kinetic properties of the associated 3'-5' exonuclease activity and its role in araAMP incorporation. J. Biol. Chem. *256*, 8525–8530. https://doi.org/10.1016/S0021-9258(19)68875-7.

72. Knopf, K.W. (1979). Properties of herpes simplex virus DNA polymerase and characterization of its associated exonuclease activity. Eur. J. Biochem. *98*, 231–244. https://doi.org/10.1111/j.1432-1033.1979.tb13181.x.

73. O'Donnell, M.E., Elias, P., Funnell, B.E., and Lehman, I.R. (1987). Interaction between the DNA polymerase and single-stranded DNA-binding protein (infected cell protein 8) of herpes simplex virus 1. J. Biol. Chem. *262*, 4260–4266. https://doi.org/10.1016/S0021-9258(18)61341-9.

74. Ostrander, M., and Cheng, Y.C. (1980). Properties of herpes simplex virus type 1 and type 2 DNA polymerase. Biochim. Biophys. Acta *609*, 232–245. https://doi.org/10.1016/0005-2787(80)90234-8.

75. Vashishtha, A.K., and Kuchta, R.D. (2016). Effects of acyclovir, foscarnet, and ribonucleotides on herpes simplex virus-1 DNA polymerase: mechanistic insights and a novel mechanism for preventing stable incorporation of ribonucleotides into DNA. Biochemistry *55*, 1168–1177. https://doi.org/10.1021/acs.biochem.6b00065.

76. Berg, O.G., Winter, R.B., and von Hippel, P.H. (1981). Diffusion-driven mechanisms of protein translocation on nucleic acids. 1. Models and theory. Biochemistry *20*, 6929–6948. https://doi.org/10.1021/bi00527a028.

77. Kalodimos, C.G., Biris, N., Bonvin, A.M.J.J., Levandoski, M.M., Guennuegues, M., Boelens, R., and Kaptein, R. (2004). Structure and flexibility adaptation in nonspecific and specific protein-DNA complexes. Science *305*, 386–389. https://doi.org/10.1126/science.1097064.

78. Santoso, Y., Joyce, C.M., Potapova, O., Le Reste, L., Hohlbein, J., Torella, J.P., Grindley, N.D.F., and Kapanidis, A.N. (2010). Conformational transitions in DNA polymerase I revealed by single-molecule FRET. Proc. Natl. Acad. Sci. USA *107*, 715–720. https://doi.org/10.1073/pnas.0910909107.

79. Lawler, J.L., Mukherjee, P., and Coen, D.M. (2018). Herpes simplex virus 1 DNA polymerase RNase H activity acts in a 3'-to-5' direction and is dependent on the 3'-to-5' exonuclease active site. J. Virol. *92*, e01813-17. https://doi.org/10.1128/JVI.01813-17.

80. Pettersen, E.F., Goddard, T.D., Huang, C.C., Couch, G.S., Greenblatt, D.M., Meng, E.C., and Ferrin, T.E. (2004). UCSF Chimera–a visualization system for exploratory research and analysis. J. Comput. Chem. *25*, 1605–1612. https://doi.org/10.1002/jcc.20084.

81. Schrödinger, L. (2015). The PyMOL Molecular Graphics System, Version 1.2r3pre (ScienceOpen.com).

82. Adams, P.D., Afonine, P.V., Bunkóczi, G., Chen, V.B., Echols, N., Headd, J.J., Hung, L.W., Jain, S., Kapral, G.J., Grosse Kunstleve, R.W., et al. (2011). The Phenix software for automated determination of macromolecular structures. Methods *55*, 94–106. https://doi.org/10.1016/j.ymeth.2011.07.005.

83. Zivanov, J., Nakane, T., Forsberg, B.O., Kimanius, D., Hagen, W.J., Lindahl, E., and Scheres, S.H. (2018). New tools for automated high-resolution cryo-EM structure determination in RELION-3. eLife *7*, e42166. https://doi.org/10.7554/eLife.42166.

84. Jones, T.A., Zou, J.Y., Cowan, S.W., and Kjeldgaard, M. (1991). Improved methods for building protein models in electron density maps and the location of errors in these models. Acta Crystallogr. A *47*, 110–119. https://doi.org/10.1107/s0108767390010224.

85. Pilger, B.D., Cui, C., and Coen, D.M. (2004). Identification of a small molecule that inhibits herpes simplex virus DNA polymerase subunit interactions and viral replication. Chem. Biol. *11*, 647–654. https://doi.org/10.1016/j.chembiol.2004.01.018.

86. Zheng, S.Q., Palovcak, E., Armache, J.P., Verba, K.A., Cheng, Y., and Agard, D.A. (2017). MotionCor2: anisotropic correction of beam-induced motion for improved cryo-electron microscopy. Nat. Methods *14*, 331–332. https://doi.org/10.1038/nmeth.4193.

87. Rohou, A., and Grigorieff, N. (2015). CTFFIND4: Fast and accurate defocus estimation from electron micrographs. J. Struct. Biol. *192*, 216–221. https://doi.org/10.1016/j.jsb.2015.08.008.

88. Wagner, T., Merino, F., Stabrin, M., Moriya, T., Antoni, C., Apelbaum, A., Hagel, P., Sitsel, O., Raisch, T., Prumbaum, D., et al. (2019). SPHIRE-crYOLO is a fast and accurate fully automated particle picker for cryo-EM. Commun. Biol. *2*, 218. https://doi.org/10.1038/s42003-019-0437-z.

89. Emsley, P., Lohkamp, B., Scott, W.G., and Cowtan, K. (2010). Features and development of *Coot*. Acta Crystallogr. D Biol. Crystallogr. *66*, 486–501. https://doi.org/10.1107/S0907444910007493.

90. Punjani, A., Rubinstein, J.L., Fleet, D.J., and Brubaker, M.A. (2017). cryoSPARC: algorithms for rapid unsupervised cryo-EM structure determination. Nat. Methods *14*, 290–296. https://doi.org/10.1038/nmeth.4169.

91. Sastry, G.M., Adzhigirey, M., Day, T., Annabhimoju, R., and Sherman, W. (2013). Protein and ligand preparation: parameters, protocols, and influence on virtual screening enrichments. J. Comput. Aided Mol. Des. *27*, 221–234. https://doi.org/10.1007/s10822-013-9644-8.

92. Bowers, K.J., Chow, E., Xu, H., Dror, R.O., Eastwood, M.P., Gregersen, B.A., Klepeis, J.L., Kolossvary, I., Moraes, M.A., Sacerdoti, F.D., et al. (2006). Scalable algorithms for molecular dynamics simulations on commodity clusters. Held in Tampa, Florida (Association for Computing Machinery).

93. Kwon, J.J., Hajian, B., Bian, Y., Young, L.C., Amor, A.J., Fuller, J.R., Fraley, C.V., Sykes, A.M., So, J., Pan, J., et al. (2022). Structure-function analysis of the SHOC2-MRAS-PP1C holophosphatase complex. Nature *609*, 408–415. https://doi.org/10.1038/s41586-022-04928-2.

94. Jorgensen, W.L., Maxwell, D.S., and Tirado-Rives, J. (1996). Development and testing of the OPLS all-atom force field on conformational energetics and properties of organicorganic liquids. J. Am. Chem. Soc. *118*, 11225–11236. https://doi.org/10.1021/ja9621760.

95. Lu, C., Wu, C., Ghoreishi, D., Chen, W., Wang, L., Damm, W., Ross, G.A., Dahlgren, M.K., Russell, E., Von Bargen, C.D., et al. (2021). OPLS4: Improving force field accuracy on challenging regimes of chemical Space. J. Chem. Theory Comput. *17*, 4291–4300. https://doi.org/10.1021/acs.jctc.1c00302.

96. Kucukelbir, A., Sigworth, F.J., and Tagare, H.D. (2014). Quantifying the local resolution of cryo-EM density maps. Nat. Methods *11*, 63–65. https://doi.org/10.1038/nmeth.2727.

97. Ter Beek, J., Parkash, V., Bylund, G.O., Osterman, P., Sauer-Eriksson, A.E., and Johansson, E. (2019). Structural evidence for an essential Fe-S cluster in the catalytic core domain of DNA polymerase ϵ. Nucleic Acids Res. *47*, 5712–5722. https://doi.org/10.1093/nar/gkz248.

98. Pettersen, E.F., Goddard, T.D., Huang, C.C., Meng, E.C., Couch, G.S., Croll, T.I., Morris, J.H., and Ferrin, T.E. (2021). UCSF ChimeraX: Structure visualization for researchers, educators, and developers. Protein Sci. *30*, 70–82. https://doi.org/10.1002/pro.3943.

99. Sievers, F., Wilm, A., Dineen, D., Gibson, T.J., Karplus, K., Li, W., Lopez, R., McWilliam, H., Remmert, M., Söding, J., et al. (2011). Fast, scalable generation of high-quality protein multiple sequence alignments using Clustal Omega. Mol. Syst. Biol. *7*, 539. https://doi.org/10.1038/msb.2011.75.

Please cite this article in press as: Shankar et al., Viral DNA polymerase structures reveal mechanisms of antiviral drug resistance, Cell (2024), https://doi.org/10.1016/j.cell.2024.07.048

STAR★METHODS

KEY RESOURCES TABLE

REAGENT or RESOURCE	SOURCE	IDENTIFIER
Bacterial and virus strains		
BL21 DE3 pLysS cells	Novagen/Millipore Sigma	Cat# 69451
Chemicals, peptides, and recombinant proteins		
α-^{32}P deoxythymidine triphosphate (dTTP)	PerkinElmer	Cat# BLU005H250UC
Deoxythymidine triphosphate (dTTP)	Invitrogen	Cat# 10219012
Acyclovir triphosphate (ACV-TP)	Jena Bioscience	Cat# NU-877
Phosphonoformic acid (PFA), trisodium salt, hexahydrate	Millipore Sigma	Cat# 1283302; CAS 34156-56-4
cOmplete™, Mini, EDTA-free protease inhibitor cocktail	Millipore Sigma	Cat# 11836170001
HSV-1 Pol (KOS strain) residues 43-1235 with an N-terminal polyhistidine tag	This paper	N/A
HSV-1 Pol (KOS strain) residues 43-1235 with W781V mutation with an N-terminal polyhistidine tag	This paper	N/A
HSV-1 UL42 (KOS strain) residues 2-340	This paper	N/A
HRV-3C protease	TaKaRa	Cat# 7360
Bromocresol green	Sigma-Aldrich	Cat# 114359
Bovine serum albumin (BSA)	Sigma-Aldrich	Cat# A7906
Amylose resin	NEB	Cat# E8021S
Deposited data		
Cryo-EM map of the HSV-1 polymerase in the open/closed conformation	This paper	EMD-42887
Cryo-EM map of HSV-1 polymerase in the editing conformation (dNTP-free class)	This paper	EMD-28664
Cryo-EM map of HSV-1 polymerase in the closed conformation bound to dTTP	This paper	EMD-42888
Cryo-EM map of HSV-1 polymerase in closed conformation bound to ACV-TP	This paper	EMD-42890
Cryo-EM map of the HSV-1 polymerase in the closed conformation bound to foscarnet	This paper	EMD-28663
Cryo-EM map of the HSV-1 polymerase in the editing conformation (mismatch-containing primer)	This paper	EMD-42889
Cryo-EM map of HSV-1 W781V Pol mutant-containing polymerase	This paper	EMD-42891
Model of the HSV-1 polymerase in the open conformation (no nucleotide)	This paper	PDB ID 8V1Q
Model of HSV-1 polymerase in the closed conformation bound to dTTP	This paper	PDB ID 8V1R
Model of HSV-1 polymerase in the closed conformation bound to ACV-TP	This paper	PDB ID 8V1T
Model of HSV-1 polymerase in the closed conformation bound to foscarnet	This paper	PDB ID 8EXX
Model of the HSV-1 polymerase in the editing conformation (mismatch-containing primer)	This paper	PDB ID 8V1S
Experimental models: Cell lines		
Sf9 cells from *Spodoptera frugiperda*	Thermo Fisher	Cat# 11496015, RRID: CVCL_JF76

(*Continued on next page*)

Please cite this article in press as: Shankar et al., Viral DNA polymerase structures reveal mechanisms of antiviral drug resistance, Cell (2024), https://doi.org/10.1016/j.cell.2024.07.048

Continued

REAGENT or RESOURCE	SOURCE	IDENTIFIER
Oligonucleotides		
Dideoxyterminated primer: 5'-GATTACGA ATTCGAGCTCGGTACCCG GGGAT/3ddC/-3' (ddC=dideoxycytosine) (from PT1 and PT2)	This paper	N/A
Mismatch containing primer with phosphorothioate modification: 5'- G*ATTACGAATTCGAGCT CGGTACCCGGGGATC*G-3' (*=phosphorothioate) (from PT3)	This paper	N/A
Template: 5'-CACACACACACAC ACACAGATCCCCGGGTACCGAGC TCGAATTCGTAATC-3' (from PT1 and PT3)	This paper	N/A
Template for ACV-TP complex: 5'-CACACACACACACACACCGATC CCCGGGTACCGAGCTCGAATTCGTA ATC-3' (from PT2)	This paper	N/A
Poly(dA)-Poly(dT)-12-18	Amersham Biosciences	Cat# 27-7868-02
Recombinant DNA		
His-UL30 ΔN42 in pFastBac HTC vector	Lawler et al.[79]	N/A
MBP-UL42 ΔC340 in pMalc2 vector	Zuccola et al.[5]	N/A
Software and algorithms		
Chimera 1.15rc	Pettersen et al.[80]	https://www.cgl.ucsf.edu/chimera/, RRID:SCR_004097
Pymol 2.5.1	Schrödinger[81]	https://pymol.org/2/, RRID:SCR_000305
Phenix 1019.2-4158	Adams et al.[82]	https://www.phenix-online.org; RRID: SCR_014224
Relion 3.1.1	Zivanov et al.[83]	https://www3.mrc-lmb.cam.ac.uk/relion/index.php/Main_Page, RRID:SCR_016274
O v15.0	Jones et al.[84]	N/A
Maestro 2022-4	Schrödinger	https://www.schrodinger.com/maestro RRID:SCR_016748

RESOURCE AVAILABILITY

Lead contact

Further information and requests for resources and reagents should be directed to and will be fulfilled by the lead contact, Jonathan Abraham (jonathan_abraham@hms.harvard.edu).

Materials availability

Unique reagents generated in this study are available from the lead contact upon request with completed material transfer agreements.

Data and code availability

- Protein Data Bank (PBD) and Electron Microscopy Data Bank (EMDB) identification numbers for the cryo-EM structures and maps reported in this manuscript are available as of the date of publication. Identification numbers are listed in the key resources table. The per-residue root-mean-square-fluctuation (RMSF) values from MD simulations reported in this study are provided in Data S2.
- This paper does not report original code.
- Any additional information required to reanalyze the data reported in this paper is available from the lead contact.

Please cite this article in press as: Shankar et al., Viral DNA polymerase structures reveal mechanisms of antiviral drug resistance, Cell (2024), https://doi.org/10.1016/j.cell.2024.07.048

EXPERIMENTAL MODEL AND STUDY PARTICIPANT DETAILS

Insect cells

Sf9 cells (*Spodoptera frugiperda*) (Thermo Fisher Scientific Cat# 11496015) cells used for recombinant HSV Pol (UL30) production were maintained in Sf-900™ II SFM (Thermo Fisher Scientific Cat# 10902088) media.

Bacterial cells

Escherichia coli BL21 (DE3) pLysS cells (Novagen Cat# 69451) were used for recombinant protein production.

METHOD DETAILS

Protein expression and purification

Wild-type KOS strain HSV Pol (UL30) (GenBank AFE62858.1) containing a 42 amino acid N-terminal deletion (HSV PolΔN42) and an N-terminal polyhistidine tag (His_6) in the pFastBac HTC was used to generate recombinant baculovirus for expression in insect cells (Sf9 cells) (Thermo Fisher Scientific Cat# 11496015).[79] Cells were infected with recombinant baculovirus and harvested 60–72 h post infection and centrifuged at 2,800 x g for 30 min. We washed pellets twice in Dulbecco's phosphate-buffered saline (DPBS) (Thermo Fisher Scientific Cat# 14190144) containing 10% (v/v) glycerol and froze pellets at -80 °C. After thawing prior to use, we resuspended cell pellets in buffer A (25 mM HEPES pH 7.5, 500 mM NaCl, 5 mM imidazole, 10% (w/v) sucrose) supplemented with protease inhibitor tablet (Millipore-Sigma Cat# 11836170001) and lysed them by sonication for 15 min (Branson Ultrasonics Sonifier Model S-450). We carried out all purification steps at 4 °C. Lysates were centrifuged at 30,000 x g for 1 h and filtered through a 0.45 μm membrane (MCE Membrane Filter) (Millipore Sigma Cat# HAWP14250). We then applied clarified supernatants onto a Hitrap™ Talon™ column (Cytiva Cat# 45-002-385) that was preequilibrated with buffer A. We washed the column with 20 column volumes of buffer A and eluted the protein using a gradient of 5 to 150 mM imidazole distributed over 20 column volumes. We collected fractions and analyzed these for purity by SDS-PAGE. Pol-containing fractions were then diluted 10-fold with H-buffer A (25mM HEPES pH 7.5, 1mM DTT and 10% sucrose (w/v)) and loaded onto a HiTrap™ Heparin HP affinity column (Cytiva Cat# 45-000-057) preequilibrated with H-buffer B (H-buffer A supplemented with 0.1 M NaCl). We washed the column with 20 column volumes of H-buffer B and eluted with a gradient of 0.1 M to 1 M NaCl over 10 column volumes. We analyzed fractions using SDS-PAGE and pooled and concentrated fractions containing HSV Pol. We dialyzed these fractions using a Slide-A-Lyzer™ MINI Dialysis Device (20K MWCO) (Thermo Scientific Cat# 88405) into storage buffer (25 mM HEPES pH 7.5, 150 mM NaCl, 2 mM tris(2-carboxyethyl)phosphine (TCEP) and 20% (v/v) glycerol).

KOS strain HSV PolΔN42 containing an N-terminal His_6 tag and the W781V mutation was generated using site-directed mutagenesis of the parent wild-type HSV PolΔN42 pFastBac™ vector. The mutant protein was expressed using recombinant baculovirus and 60–72 hours post-infection, Sf9 cells were harvested and sonicated as noted above with WT HSV Pol. The clarified supernatant was then applied onto Ni Sepharose™ excel (Cytiva Cat# 45-003-011). The column was washed with 50 column volumes of buffer A and the protein was eluted using buffer A supplemented with 250 mM imidazole (25 mM HEPES pH 7.5, 500 mM NaCl, 10% (w/v) sucrose, 250 mM imidazole) over 20 column volumes. The eluted protein was then diluted 10-fold with H-buffer A and loaded onto a HiTrap™ Heparin HP affinity column, with purification performed as noted above with WT HSV Pol. Purified UL30 W781V was concentrated and dialyzed into storage buffer, then frozen at -80 °C for future use.

We expressed a UL42 (GenBank AFE62870) construct containing an N-terminal maltose binding protein (MBP) tag followed by a PreScission protease cleavage site and residues 2–340 of UL42 (MBP-UL42ΔC340) in *Escherichia coli* BL21 (DE3) pLysS cells (Novagen Cat# 69451) and generated purified tag-less protein.[5,54] We grew cells that were transformed with the MBP-UL42 ΔC340 in pMalc2 vector in Luria-Bertani (LB) broth with 2% (w/v) glucose in presence of ampicillin at 100 μg ml^{-1} and chloramphenicol at 25 μg ml^{-1} for selection. Cells were induced with 0.3 mM isopropyl β-D-1-thiogalactopyranoside (IPTG) at OD_{600} ~0.6–0.8 and allowed to grow overnight at 16 °C. We harvested cells by centrifugation at 4000 x g for 30 min and resuspended them in M-buffer A (25 mM HEPES pH 7.5, 500 mM NaCl, 1 mM EDTA, 1mM DTT, and protease inhibitor (cOmplete™, Mini, EDTA-free protease inhibitor cocktail, Millipore Sigma, Cat# 11836170001)). We lysed cells by sonication for 15 min (Branson Ultrasonics Sonifier Model S-450). We then centrifuged lysates for 90 min at 18,000 x g at 4 °C and applied supernatants to amylose resin (NEB Cat# E8021S). We washed the column with M-buffer A for 10–15 column volumes, eluted protein with M-buffer B (M-buffer A +10 mM maltose) and analyzed fractions by SDS-PAGE. We pooled fractions and diluted these with H-buffer A to reduce the effective NaCl concentration to 150 mM. We cleaved the MBP-tag by adding polyhistidine-tagged HRV-3C protease (TaKaRa Cat# 7360) at 4 °C overnight and passed samples over a HiTrap TALON® crude column (Cytiva Cat # 28953809) to remove the protease. We applied flowthrough from this step onto HiTrap™ Heparin HP affinity column preequilibrated with H-buffer B. The column was washed with 20 column volumes of H-buffer B and eluted with a gradient of 0.1M to 1M NaCl over 10 column volumes. Fractions were pooled and stored in storage buffer.

DNA elongation assays

Long-chain DNA synthesis by HSV PolΔN42 and UL42 on a poly(dA)-oligo(dT)12-18 primer-template (Amersham Biosciences Cat# 27-7868-02) with α-^{32}P deoxythymidine triphosphate (dTTP) (Perkin Elmer Cat# BLU005H250UC) was measured using a gel-based

Please cite this article in press as: Shankar et al., Viral DNA polymerase structures reveal mechanisms of antiviral drug resistance, Cell (2024), https://doi.org/10.1016/j.cell.2024.07.048

assay described previously[85] with the following minor modifications: reaction mixtures containing 50 mM Tris-HCl pH 7.5, 100 mM $(NH_4)_2SO_4$, 3 mM $MgCl_2$, 0.1 mM EDTA, 1 mM 1,4-dithiothreitol (DTT), 4% (v/v) glycerol, 40 μg ml^{-1} bovine serum albumin (BSA), 26 μg ml^{-1} primer-template, 50 μM [α-^{32}P]dTTP (~55 Ci/mmol) and 50 μM dTTP were supplemented with 12 nM of HSV Pol alone or with 12, 24, or 48 nM UL42, respectively. Reactions were carried out at 37°C for 10 min and were stopped by the addition of alkaline loading dye (2 mM EDTA, 50 mM NaOH, 2.5% (v/v) glycerol, 0.025% (w/v) Bromocresol green, Sigma-Aldrich Cat# 114359) and immediate incubation on ice. Samples were loaded onto a 4% alkaline agarose gel, and, after electrophoresis, gels were dried overnight and exposed to phosphorescence screens (Bio-Rad), followed by scanning using a Bio-Rad Personal Molecular Imager. The results of the DNA elongation assay are provided in Figure S1A.

Long-chain DNA synthesis assays of WT and the W781V HSV PolΔN42 mutant were performed using a M13mp18 ssDNA template (NEB Cat# N4040S) with 5' 6-Carboxyfluorescein (6-FAM) labeled M13 forward primer (Integrated DNA Technologies) and were measured using a gel-based assay described previously[85] with the following minor modifications: reaction mixtures containing 50 mM Tris-HCl pH 7.5, 100 mM $(NH_4)_2SO_4$, 8 mM $MgCl_2$, 0.1 mM EDTA, 1 mM 1,4-dithiothreitol (DTT), 4% (v/v) glycerol, 40 μg ml^{-1} bovine serum albumin (BSA), 25 μg ml^{-1} primer-template, 1.2mM dNTP were supplemented with 40 nM W781V HSV PolΔN42 or wild-type HSV PolΔN42 (control) with or without 64 nM of UL42. Reactions were carried out at 37°C for 2 hr and were stopped by the addition of loading dye (0.05% [v/v] bromophenol blue, 0.05% [v/v] xylene cyanol, 80% [v/v] formamid, 100 mM EDTA) and immediate incubation on ice. Samples were loaded onto a 10% acrylamide DNA sequencing gel, and, after electrophoresis, gels were exposed to Typhoon FLA 9000 Gel Imaging Scanner (GE) at Alexa 488. The results of a DNA elongation assay with WT and W781V mutant HSV Pol are provided in Figure S7D.

Cryo-EM sample preparation

All samples for cryo-EM were prepared with a Vitrobot Mark IV (Thermo Fisher Scientific), with samples maintained at 100% humidity at room temperature. DNA primer-template sequences are provided in Figure S1B. Sample conditions for each of the complexes were as follows: HSV polymerase holoenzyme without nucleotide, ~7 μM HSV Pol-UL42-DNA primer-template (PT1) complex in buffer containing 25 mM HEPES pH 7.5 and 150 mM NaCl; HSV-1 polymerase holoenzyme with dTTP, ~7 μM HSV Pol-UL42-DNA primer-template (PT1) complex and 7 μM of deoxythymidine triphosphate (dTTP, Invitrogen Cat# 10219012) in buffer containing 25 mM HEPES pH 7.5 and 150 mM NaCl; HSV-1 polymerase holoenzyme bound to ACV-TP, ~7 μM HSV Pol-UL42-DNA primer-template (PT2) complex and 7 μM of ACV-TP (Jena Bioscience; Cat# NU-877) in buffer containing 25 mM HEPES pH 7.5 and 150 mM NaCl; HSV-1 polymerase holoenzyme bound to foscarnet, ~7 μM HSV Pol-UL42-DNA primer-template (PT1) complex and 7 μM of foscarnet (phoshonoformic acid, Millipore Sigma Cat# 1283302) in buffer containing 25 mM HEPES pH 7.5 and 150 mM NaCl; HSV polymerase holoenzyme with mismatch-containing primer, ~7 μM HSV Pol-UL42-DNA primer-template (PT3) complex in buffer containing 25 mM HEPES pH 7.5, 150 mM NaCl (in addition, to decrease exonuclease-mediated primer end cleavage, the PT3 primer ends contained phosphorothioate bonds and 2 mM EDTA was added to the buffer); HSV-1 polymerase holoenzyme with W781V Pol mutant, ~7 μM HSV Pol W781V-UL42-DNA primer-template (PT1) in buffer containing 25 mM HEPES pH 7.5 and 150 mM NaCl. DNA primer-template sequences are provided in Figure S1B. We applied 3 μl of samples to Quantifoil Cu 1.2/1.3 400 mesh (EMS Cat# Q450CR1.3) or Quantifoil Cu 2.0/1.0 400 mesh (EMS Cat# Q450CR1) grids that were previously plasma treated in a Pelco easiGlow™ discharge cleaning system at 0.39 mBar, 15 mA, for 30 s and used blot times of 5–10 s.

Cryo-EM data collection

For the dataset of HSV Pol/UL42/DNA primer-template complex with or without dTTP, with ACV-TP, with foscarnet, and for the editing polymerase complex with mismatch containing DNA primer-template, we collected datasets on a Cs-corrected Titan Krios (Thermo Fisher Scientific) operating at 300 kV, with post-GIF energy filter (20 eV slit) and a Gatan K3 camera in counting mode at 105,000 x magnification, corresponding to calibrated pixel size of 0.825 Å/pixel. For the dataset of HSV Pol/UL42/DNA primer-template complex without nucleotide, 6173 movies were collected at a dose rate of 26.5 e^- $pixel^{-1}$ s^{-1}. The total exposure time of 1.5 s was divided into 38 frames (total dose of approximately 53.1 ($e^-/Å^2$)). For the dataset of HSV Pol/UL42/DNA primer-template complex with dTTP, 3855 movies were collected at a dose rate of 26.9 e^- $pixel^{-1}$ s^{-1}. The total exposure time of 2.1 s was divided into 38 frames (total dose of approximately 56.5 $e^-/Å^2$). For the dataset of HSV Pol/UL42/DNA primer-template complex with ACV-TP, we collected 3272 movies with 50 frames per movie, at a total dose of 53 e^- $/Å^2$. For the dataset of HSV Pol/UL42/DNA primer-template complex with foscarnet, we collected 4914 movies with 50 frames per movie, at a total dose of 53.9 e^- $/Å^2$. For the HSV Pol/UL42 mismatch-containing DNA primer-template editing complex, we collected 5076 movies at a dose rate of 15.05 e^- $pixel^{-1}$ s^{-1}. The total exposure time of 2.5 s was divided into 50 frames (total dose of approximately 55.2 $e^-/Å^2$). For the HSV Pol W781V mutant/UL42/DNA primer-template complex, we collected 1678 movies at a dose rate of 23.06 e^- $pixel^{-1}$ s^{-1}. The total exposure time of 2.5 s was divided into 50 frames (total dose of approximately 57.6 $e^-/Å^2$). A defocus range of -1.0 μm to -2.5 μm was used in all cases. The objective and C2 apertures were set to 100 μm and 50 μm respectively.

Cryo-EM image processing

We performed all image processing using Relion 3.0.[83] Movie frames were gain-normalized and motion-corrected using MotionCor2.[86] Contrast transfer function (CTF) correction was performed using CTFFind4.1,[87] as implemented in Relion 3.0. We performed automated particle-picking in crYOLO.[88] Picked particles were imported to Relion, extracted, binned to a pixel size of 3.3 Å and

Please cite this article in press as: Shankar et al., Viral DNA polymerase structures reveal mechanisms of antiviral drug resistance, Cell (2024), https://doi.org/10.1016/j.cell.2024.07.048

subjected to 2D classification. Good classes of particles from the 2D classification were selected and subjected to 3D classification using ~8 Å map generated from data collected at 200 kV Tecnai F20 equipped with a Gatan K2 summit camera as an initial model.

For datasets collected on HSV Pol/UL42/DNA primer-template complex without nucleotide, a subset of particles (343,777 in total) generated from rounds of 3D classification of 1,101,138 particles that appeared to adopt the open conformation was subjected to masked refinement and polishing/CTF refinement, yielding a final map of 2.7 Å with improved density (Figure S1C; Table S1). Despite several attempts, we could not detect separate sets of particles either adopting the open and closed conformations in the final particle subclass using signal subtraction or additional rounds of subparticle classification in Relion. This is likely because the differences in conformation only involved the two α-helices in the fingers domain. Some of the 3D classes generated during the first round of 3D classification of particles included 580,672 particles that appeared to favor the editing conformation. Additional 3D classification and auto-refinement of one subclass (including 125,216 particles in total) yielded a final map of 3.8 Å (Figure S1C; Table S1).

For the HSV Pol/UL42/DNA primer-template complex with dTTP, a subset of particles (473,353 in total) generated from rounds of 3D classification were combined and subjected to auto-refinement, masked refinement, and polishing/CTF refinement to generate a final map of 2.8 Å (Figure S3A; Table S1). For the HSV Pol/UL42/DNA primer-template complex with ACV-TP, a subset of particles (187,300 in total) generated from rounds of 3D classification were subjected to auto-refinement, masked refinement, and polishing/CTF refinement to achieve a final resolution of 2.8 Å (Figure S3B). For the HSV Pol/UL42/DNA primer-template complex with foscarnet, a subset of particles (264,472 in total) generated from rounds of 3D classification followed by auto-refinement, masked refinement, and CTF refinement/polishing yielded a final map with an average resolution of 3.3 Å (Figure S3C; Table S1).

To obtain higher resolution maps for an editing polymerase complex, a DNA primer-template pair with a mismatch was used to bias particles towards this conformation and a phosphorothioate bond was introduced between the penultimate nucleotides primer 5' and 3' termini (see Figure S1B) to stabilize the primer and template against 3'-5' exonuclease activity. A subset of particles (362,860 particles) was subjected to auto-refinement. The density of DNA was further improved by subtracting the protein signal, followed by 3D classification, and refinement, yielding final maps of 3.3 Å (Figure S7A; Table S1). For HSV Pol W781V mutant/UL42/DNA primer-template complex, a subset of particles (232,946 particles) generated from a round of 3D classification followed by auto-refinement, masked refinement, and CTF refinement/polishing yielded a final map with an average resolution of 5.1 Å (Figure S7E).

Model building and refinement

The crystal structure of HSV pol (PDB: 2GV9)[4] and UL42 (PDB: 1DML)[5] were fitted as rigid bodies into cryo-EM map using Chimera.[80] Although cryo-EM maps in the UL42 region were lower in quality than they were at the Pol core and the quality of the UL42 density varied in the multiple structures, likely due to flexibility, the high-resolution X-ray crystal structure of a UL42/Pol C-terminal peptide complex (2.7 Å)[5] could be unambiguously docked and used as a starting point for model building in all of the structures. UL42 residues 2–28 and 228–251, which were disordered in the X-ray crystal structure of UL42 alone,[5] could also not be visualized in cryo-EM maps of the complexes. We performed manual adjustments and iterative model building and real space refinement using *Coot*[89] and PHENIX.[82] Figures were generated using PyMol and UCSF Chimera.[80] To model the alternate, closed fingers conformation shown in Figure 1B, we fit the closed conformation polymerase structure into maps collected for the polymerase in the absence of nucleotide (see Figure S1D), and the fingers fit the density corresponding to the alternative conformation nearly perfectly, whereas the rest of Pol was nearly identical to the equivalent parts in the open structure, with an all-atom RMSD of only 0.33 Å. For map interpretation, the 3.3 Å map of the editing holoenzyme bound to DNA primer-template with a mismatch was docked into the 5.1 Å map of the mutant holoenzyme (Figure S7F). DNA template residues -4 to -7 in the ssDNA binding groove could be modeled and were used during figure generation but were not included in deposited coordinates because they were associated with weak density.

3D variability analysis

3D variability analysis (3DVA) was performed on the data set with HSV Pol/UL42/DNA primer-template complex in the absence of nucleotide using cryoSPARC.[22,90] Particle stacks and reference map from Relion were imported and a consensus refinement was performed using homogenous refinement. Two separate instances of 3DVA were performed, one using a mask generated from homogenous refinement and the other following a heterogenous refinement. The first instance, which we carried out on all good particles (and not a particular subclass), generated three components, of which the major component showed flexibility in the DNA. In the second instance, two rounds of heterogeneous refinement were performed and selected particles from a subclass (~60%, thought to represent the open/closed conformation) were subjected to 3DVA using a mask generated from heterogeneous refinement. In this second instance, a major component showed movement in the fingers domain. The frames from these components were visualized and recorded in UCSF Chimera[80] as a volume series (see Video S1).

In silico modeling and MD simulations

The cryo-EM structures of the HSV Pol/UL42/DNA primer-template complex without nucleotide (open conformation), with dTTP (closed conformation), with ACV-TP, and with foscarnet were prepared before modelling and simulations. The module of Protein Preparation in Schrödinger Maestro[91] was applied to cap termini, repair residues, optimize H-bond assignments, and run restrained minimizations following default settings. *In silico* mutations of E597K, A605V, L774F, and W781V for open and closed conformations,

and an *in silico* mutation of W781V for drug bound structures, were realized using the module of 3D Builder in Schrödinger Maestro. Protein models after the *in silico* mutations underwent the same preparation procedure.

The Schrödinger Desmond MD engine[92] was used for simulations as previously described.[93] An orthorhombic water box was applied to bury prepared protein systems with a minimum distance of 10 Å to the edges from the protein. Water molecules were described using the SPC model. Na^+ ions were placed to neutralize the total net charge. All simulations were performed following the OPLS4 force field.[94,95] The ensemble class of NPT was selected with the simulation temperature set to 300K (Nose-Hoover chain) and the pressure set to 1.01325 bar (Martyna-Tobias-Klein). A set of default minimization steps pre-defined in the Desmond protocol was adopted to relax the MD system. Position restraints were applied towards the DNA. The simulation time was set to 100 ns for each protein system (WT open, WT closed, E597K open, E597K closed, A605V open, A605V closed, L774F open, L774F closed, W781V open, W781V closed, WT closed with dTTP deletion, W781V closed with dTTP deletion, WT with ACV-TP, WT with ACV-TP deletion, WT with foscarnet, WT with foscarnet deletion, W781V with ACV-TP, and W781V with foscarnet). Each protein system underwent three duplicate MD runs. One frame was recorded per 200 ps during the sampling phase. Post-simulation analysis of the RMSF was performed using a Schrödinger simulation interaction diagram. Representative frames for each mutated protein system were selected using the function of Trajectory Frame Clustering in Schrödinger Maestro. Up to 5 clusters were reported based on a RMSD matrix of the Cα atoms of residues. The centroid of the most populated cluster was reported as a representative. Data for RMSF fluctuations are provided in Data S2.

QUANTIFICATION AND STASTICAL ANALYSIS

The data analysis function in Microsoft Excel (version 16.62) was used to conduct the unpaired, two-tailed Student's t-test to compare mean RMSF values from two groups. The details of tests, including the number of replicates, are included in figure legends. Statistical significance was defined as $p < 0.05$.

CellPress
OPEN ACCESS

Supplemental figures

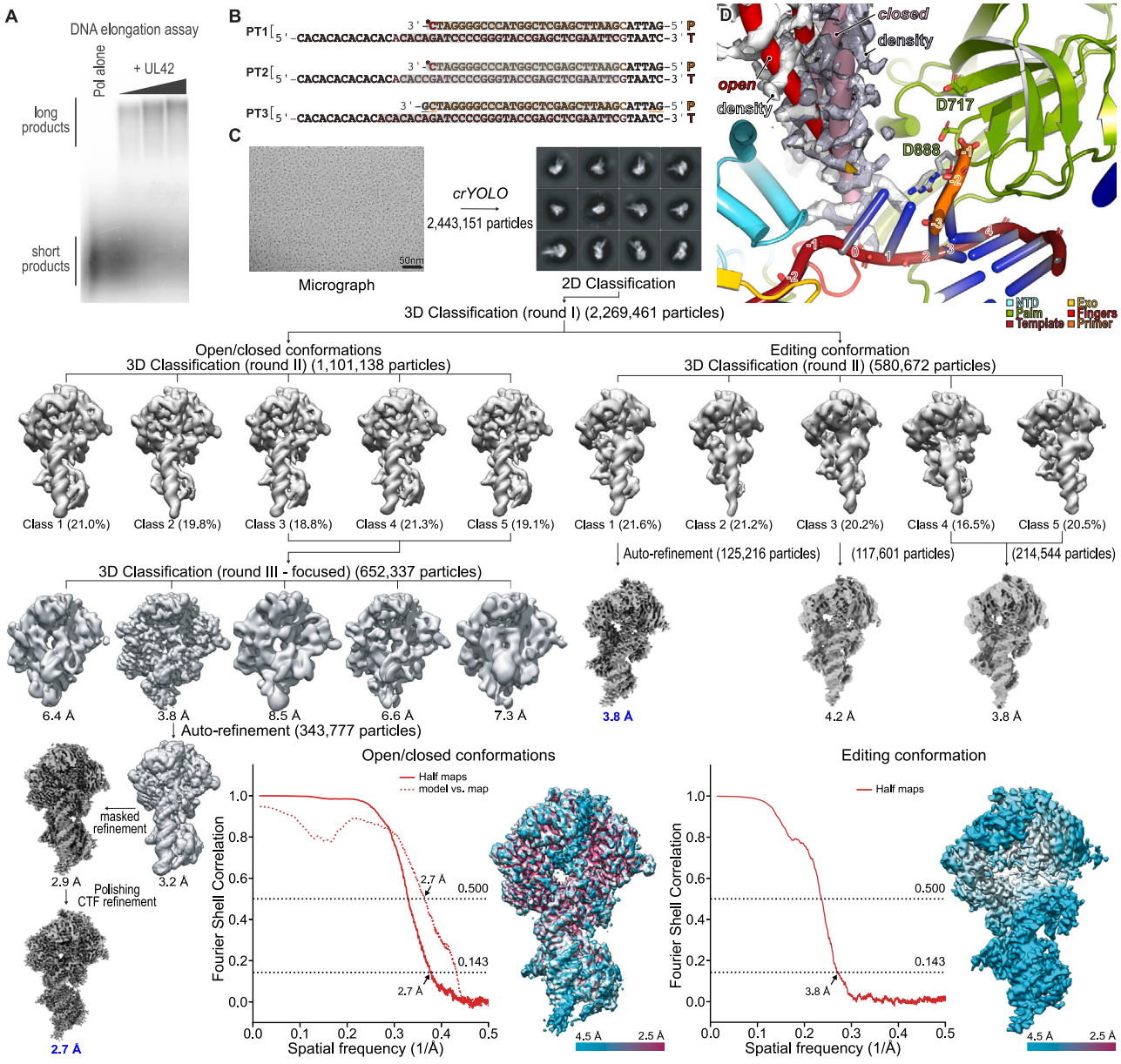

Figure S1. Structure determination workflow for the DNA-bound HSV polymerase in the absence of nucleotide, related to Figure 1

(A) Long-chain DNA synthesis by HSV Pol in the absence or presence of different concentrations of UL42. Lane 1, HSV Pol alone; lanes 2–4, HSV Pol with UL42 at a molar ratio of 1:1, 1:2, and 1:4, respectively. Reactions were visualized by incorporation of radiolabeled dTTP into a poly(dA)-oligo(dT) primer-template followed by alkaline agarose gel electrophoresis.

(B) Sequences for primer-template DNA used in our studies. Nucleotides labeled with an asterisk are dideoxy-terminated to prevent elongation. P, primer. T, template. Bases that are underlined in PT3 are linked by a phosphorothioate bond to decrease exonuclease-mediated cleavage. Nucleotides visualized in cryo-EM structures are shaded gray.

(C) Flow chart depicting the cryo-EM data processing workflow for determining the structure of the DNA primer-template-bound (PT1) HSV polymerase collected without nucleotide. The resolutions of maps that were used for further structural analysis are indicated in blue, and Fourier shell correlation plots are provided for these maps. Estimates of local resolution were determined using ResMap.[96] Additional information is provided in the STAR Methods.

(D) Zoom-in view of the Pol active site for the HSV polymerase holoenzyme bound to DNA primer-template in the absence of nucleotide. Density for both the open (white) and closed (gray) fingers was observable in cryo-EM maps contoured at the same level.

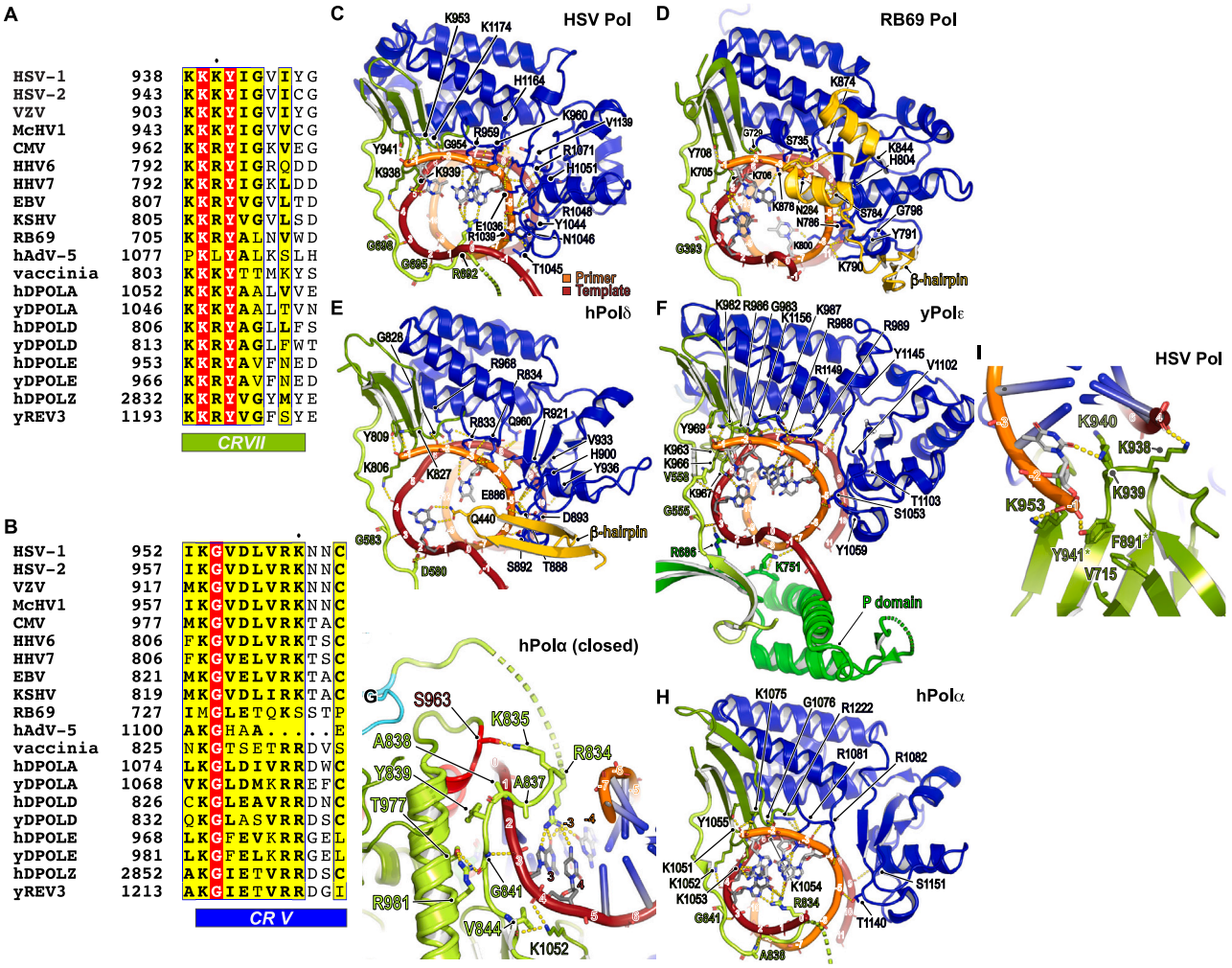

Figure S2. HSV Pol palm and thumb DNA contacts and comparison with other B-family DNA polymerases, related to Figure 2

(A) Sequence alignment of Pol CRVII showing the location of the conserved KK(K/R)Y motif (HSV-1 residues 938–941) in the palm.

(B) Sequence alignment of CRV in the Pol thumb.

(C) View showing contacts HSV Pol CRVII, CRV, and the palm-NTD loop make with DNA.

(D) Similar view of the Pol region shown in (C) but instead with RB69 gp43 Pol (PDB: 1IG9).[19]

(E) Similar view of the HSV Pol region shown in (C) but instead with human Pol δ (hPolδ) (PDB: 6TNY).[15]

(F) Similar view of the HSV Pol region shown in (C) but instead with yeast Pol ϵ (yPolϵ) (PDB: 6H1V).[97] The P domain (shown in a different shade of green) involves different palm loops, helps encircle the DNA, and has been suggested to influence processivity.[20]

(G) Zoom-in view highlighting human Pol α (hPolα) (PDB: 6AS7)[21] DNA contacts in the region that is analogous to the one in which the HSV Pol palm-NTD loop contacts DNA (see Figure 2B). Interactions the hPolα R834 side chain makes with bases on the primer and template strands are similar to contacts that HSV $R692_{Pol}$ make with bases on the template and primer. Additionally, the side chain of hPolα R981, like that of HSV $R842_{Pol}$, makes contacts that tether the loop to an α-helix in the palm.

(H) Similar view of the HSV Pol region shown in (C) but instead with hPolα (PDB: 6AS7).

(I) Contacts $Y941_{Pol}$ makes with the primer 3′ end. The Y941H and F891C substitutions confer resistance to acyclovir and foscarnet (these mutated residues are indicated with asterisks). The mutations would compromise proper positioning of the primer end, reducing stability of the ternary complex.

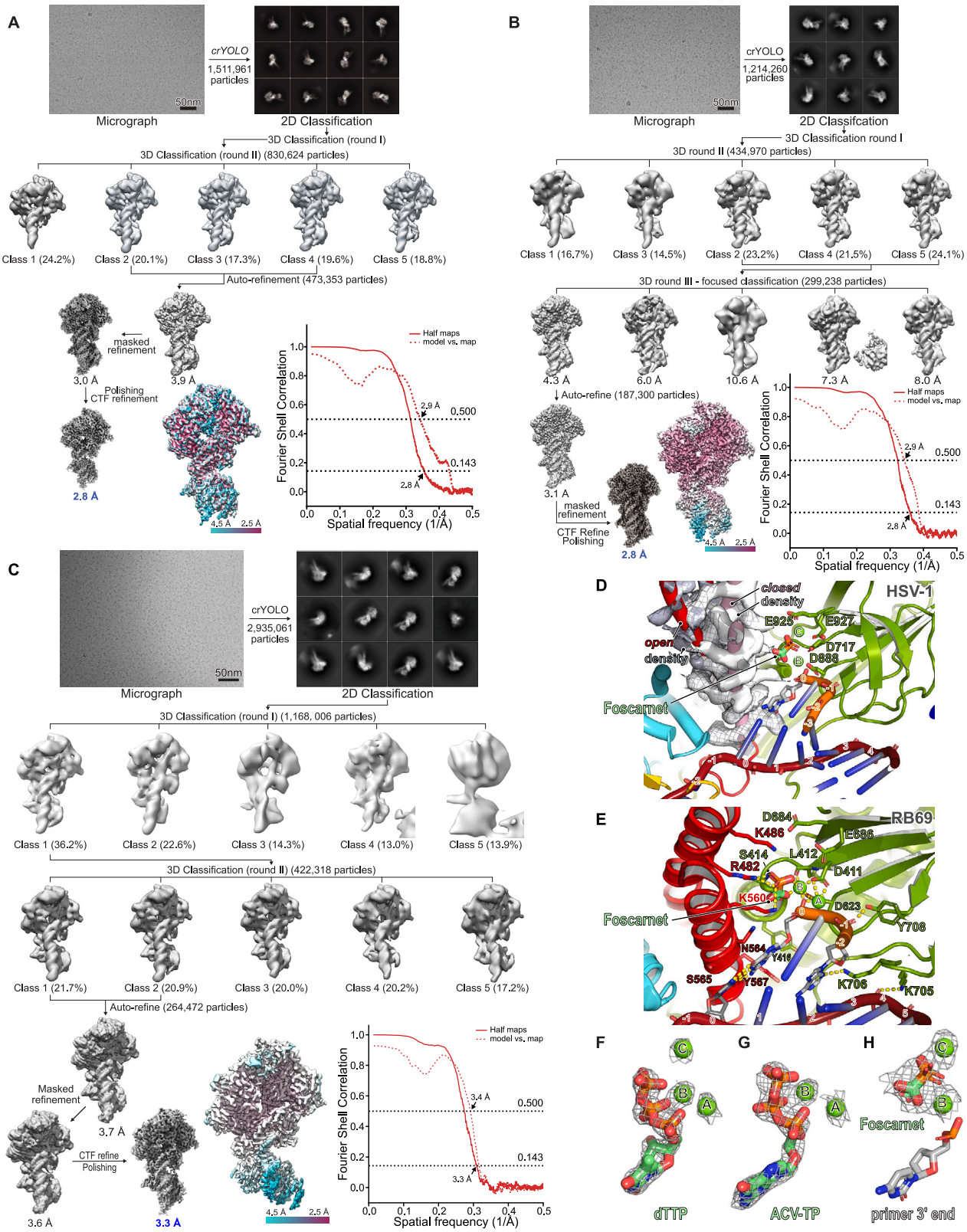

(legend on next page)

Figure S3. Structure determination workflows for DNA-bound HSV polymerase with dTTP, ACV-TP, and foscarnet, related to Figure 3

(A–C) Flow chart depicting the cryo-EM data processing workflow for determining the structure of the DNA primer-template-bound (PT1) HSV polymerase with dTTP (A), the structure of the DNA primer-template (PT2)-bound HSV polymerase with ACV-TP (B), or the structure of the DNA primer-template-bound (PT1) HSV polymerase with foscarnet (C). The resolutions of maps used for structural analysis are indicated in blue, and Fourier shell correlation plots are provided for these maps. Estimates of local resolution were determined using ResMap.[96] Additional information is provided in the STAR Methods.

(D) Pol active site for the HSV polymerase holoenzyme bound to DNA primer-template in the presence of foscarnet. Weak density for the open (gray) and strong density for the closed (white) fingers was observable in cryo-EM maps contoured at the same level.

(E) Zoom-in view of the active site of the previously determined X-ray crystal structure of an engineered mutant bacteriophage RB69 gp43 (Pol) fingers domain mutant bound to foscarnet (PDB: 3KD5).[69] The complex includes an acyclovir terminated primer 3′ end, which is untranslocated in the structure. Residue K486 in RB69 gp43 corresponds to residue R789 in HSV Pol.

(F) Cryo-EM density for dTTP and metals in the 2.8 Å map of dTTP-bound HSV polymerase. The density for metal C is weaker, so a lower contour level than that used for metals A and B was used here to visualize it.

(G) Cryo-EM density for ACV-TP and metals in the 2.8 Å map of ACV-TP-bound HSV polymerase.

(H) Cryo-EM density for foscarnet and metals in the 3.3 Å cryo-EM structure of foscarnet-bound HSV polymerase holoenzyme. The dideoxy-terminated primer 3′ end is also shown.

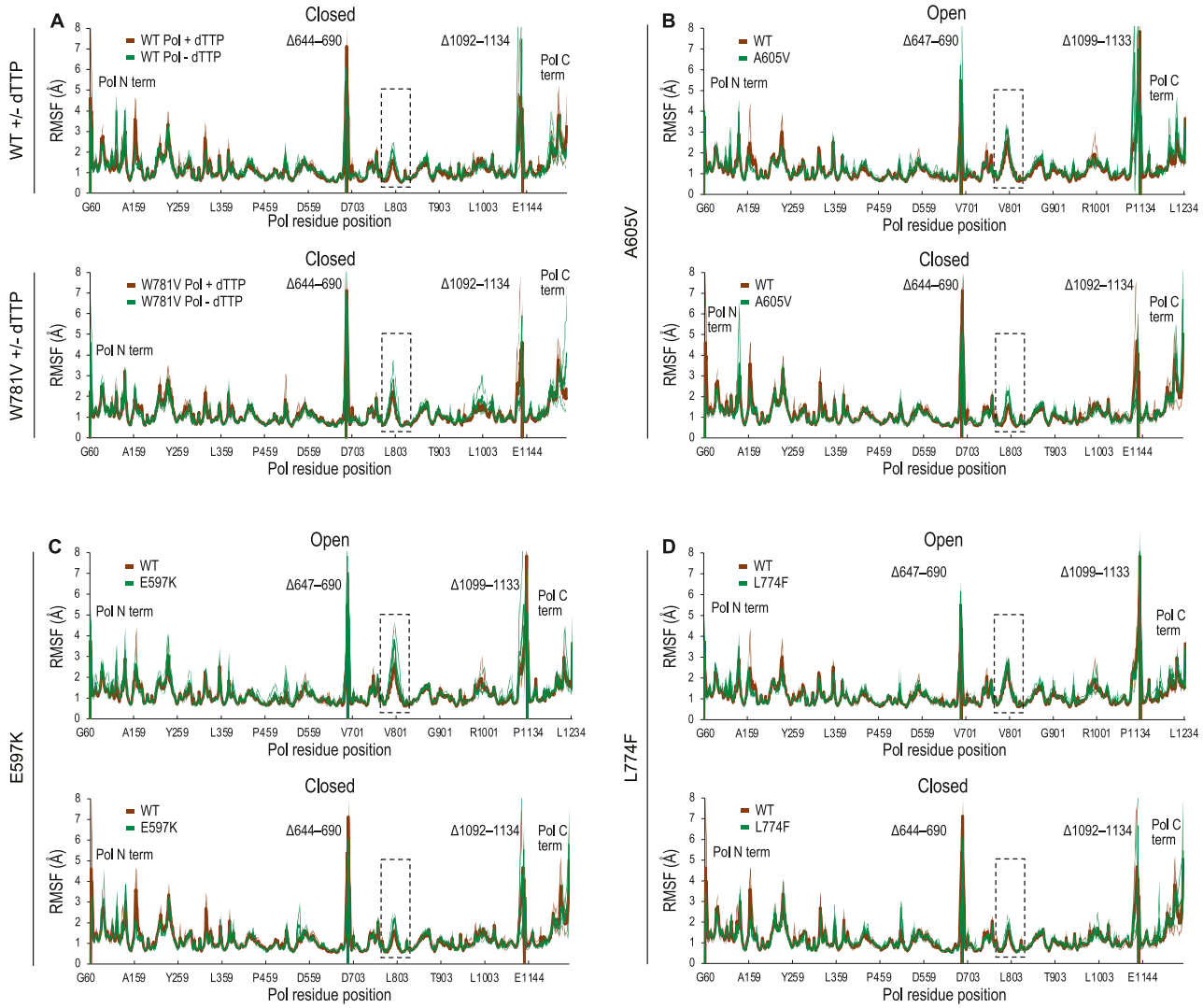

Figure S4. Full tracings for per-residue fluctuation of wild-type and mutant Pols, related to Figures 4 and S5

(A) Per-residue root-mean-square-fluctuation (RMSF) reflected from 100 ns MD simulations of the wild-type (WT) holoenzyme in the closed conformation in the presence of absence of dTTP (top) or W781V mutant in the presence or absence of dTTP (bottom).

(B–D) Per-residue RMSF reflected from 100 ns MD simulations of the holoenzyme in the open (top) or closed (bottom) conformations for WT Pol and the A605V Pol mutant (B), the E597K Pol mutant (C), or the L744F mutant (D).

In all panels, fingers domain residues are shown in dashed boxes.

Regions denoted Δ are absent in models (lacked interpretable density in cryo-EM maps).

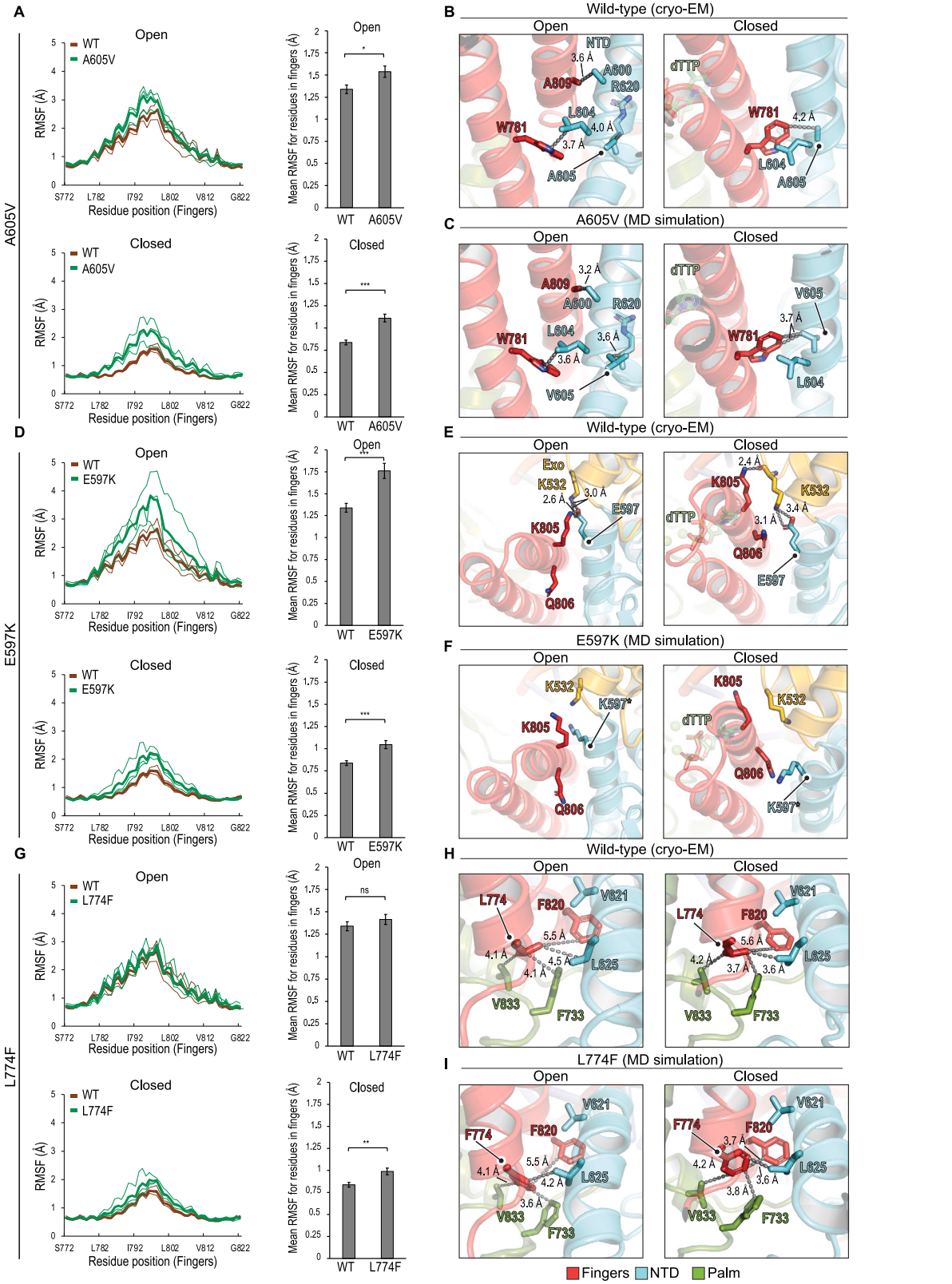

(legend on next page)

Figure S5. Effects of additional drug-resistance mutations on structural fluctuations in the fingers domain, related to Figure 4

(A) Per-residue root-mean-square-fluctuation (RMSF) of fingers domain residues reflected from 100 ns MD simulations of the polymerase in the open (top left) or closed (bottom left) conformations for wild type (WT) or the A605V Pol mutant. Statistical assessment of RMSF values for fingers domain residues was plotted for the open (top right) and closed (bottom right) conformations for the WT and mutated Pol.

(B) View of fingers domain residue A605 and neighboring residues in the open or dTTP-bound closed conformations as determined from cryo-EM structures.

(C) View of representative frames from the 100 ns MD simulations to show neighboring residues for the A605V mutant enzyme in the open and closed conformations.

(D) Per-residue RMSF of fingers domain residues reflected from 100 ns MD simulations of the holoenzyme in the open (top) or closed (bottom) conformation for WT Pol and the E597K Pol mutant. Statistical assessment of RMSF values for fingers domain residues was plotted for the open (top right) and closed (bottom right) conformations for WT and mutated Pol.

(E) View of NTD residue E597 and neighboring residues in the open or dTTP-bound closed conformations as determined from the cryo-EM structures.

(F) Representative frame from the 100 ns MD simulations to show neighboring residues for the E597K mutant enzyme in the open or closed conformations.

(G) Per-residue fluctuation of the fingers domain reflected from 100 ns MD simulations of the holoenzyme in the open (top) or closed (bottom) conformation for WT Pol and the L774F mutant. Statistical assessment of RMSF values for fingers domain residues was plotted for the open (top right) and closed (bottom right) conformations for the WT and mutated Pol.

(H) View of fingers domain residue L774 and neighboring residues in the open or dTTP-bound closed conformations as determined from the cryo-EM structures.

(I) Representative frame from the 100 ns MD simulations to show neighboring residues for the L774F mutant enzyme in the open or dTTP-bound closed conformations.

For panels shown in (A), (D), and (G), full RMSF tracings are provided in Figure S4, and the comparison between two groups was performed using an unpaired, two-tailed Student's t test. Error bars represent standard errors. $*p < 0.05$, $**p < 0.01$, and $***p < 0.001$. ns, no statistical significance.

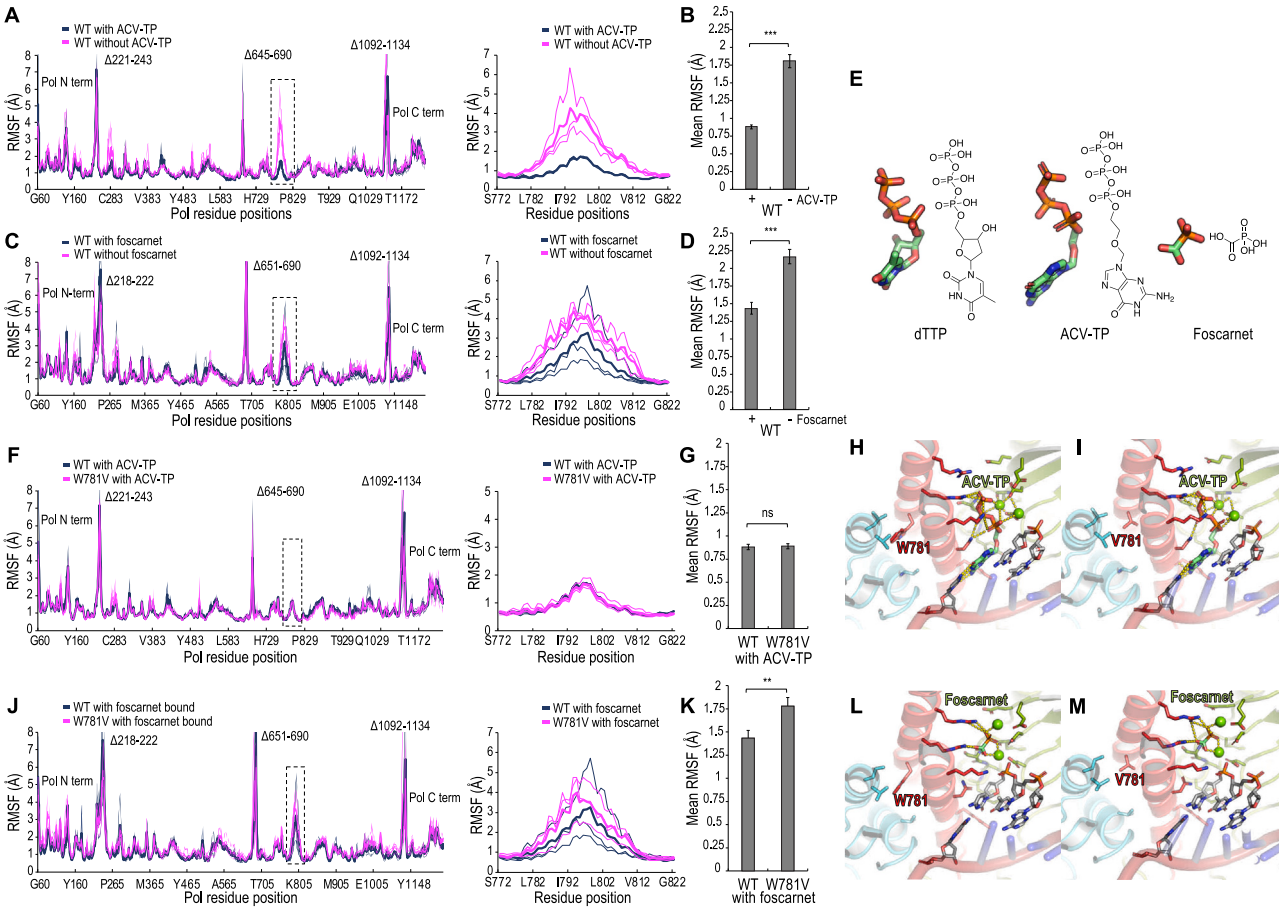

Figure S6. Molecular dynamics simulations of HSV polymerase with and without antivirals, related to Figure 4

(A) Per-residue root-mean-square-fluctuation (RMSF) from MD simulations of the polymerase with ACV-TP occupying the active site (cryo-EM, blue trace) and the ACV-TP deleted structure (modeled, pink trace).

(B) Mean RMSF values calculated during MD simulations for fingers residues (S772–G822) are plotted for the ACV-TP bound (cryo-EM) and ACV-TP deleted (modeled) structures. Comparison of mean RMSF values between the two groups was performed using an unpaired, two-tailed Student's t test. Error bars represent standard errors. ***$p < 0.001$.

(C) Per-residue RMSF from MD simulations of the polymerase with foscarnet occupying the active site (cryo-EM, blue trace) and the foscarnet deleted structure (modeled, pink trace).

(D) Mean RMSF values calculated during MD simulations for fingers residues (S772–G822) are plotted for the foscarnet-bound (cryo-EM) and foscarnet-deleted (modeled) structures. The comparison of mean RMSF values between two groups was performed using an unpaired, two-tailed Student's t test. Error bars represent standard errors. ***$p < 0.001$.

(E) Structures of dTTP, ACV-TP, and foscarnet in 3D (shown as sticks) and 2D.

(F) Per-residue root-mean-square-fluctuation (RMSF) from MD simulations of WT HSV Pol with ACV-TP occupying the active site (cryo-EM, blue trace) and the HSV Pol W781V holoenzyme with ACV-TP occupying the active site (modeled, pink trace).

(G) Mean RMSF values calculated during MD simulations for fingers residues (S772–G822) are plotted for WT HSV Pol holoenzyme with ACV-TP occupying the active site and the HSV Pol W781V holoenzyme with ACV-TP occupying the active site. The comparison of mean RMSF values between two groups was performed using an unpaired, two-tailed Student's t test. ns, not significant.

(H and I) Views of the Pol active site in the presence of acyclovir triphosphate (ACV-TP) showing the location of W781 (H) or V781 (modeled) (I) at the NTD-fingers domain interface. Selected contacts for the ACV-TP are shown as yellow dashes. Metals are shown as green spheres.

(J) Per-residue root-mean-square-fluctuation (RMSF) from MD simulations of the WT HSV Pol holoenzyme with foscarnet occupying the active site (cryo-EM, blue trace) and the HSV Pol W781V holoenzyme with foscarnet occupying the active site (modeled, pink trace).

(K) Mean RMSF values calculated during MD simulations for fingers residues (S772–G822) are plotted for WT HSV Pol holoenzyme with foscarnet occupying the active site and the HSV Pol W781V holoenzyme with foscarnet occupying the active site. The comparison of mean RMSF values between two groups was performed using an unpaired, two-tailed Student's t test. **$p < 0.01$.

(L and M) Views of the Pol active site in the presence of foscarnet showing the location of W781 (L) or V781 (modeled) (M) at the NTD-fingers domain interface. Selected contacts for foscarnet are shown as yellow dashes. Metals are shown as green spheres.

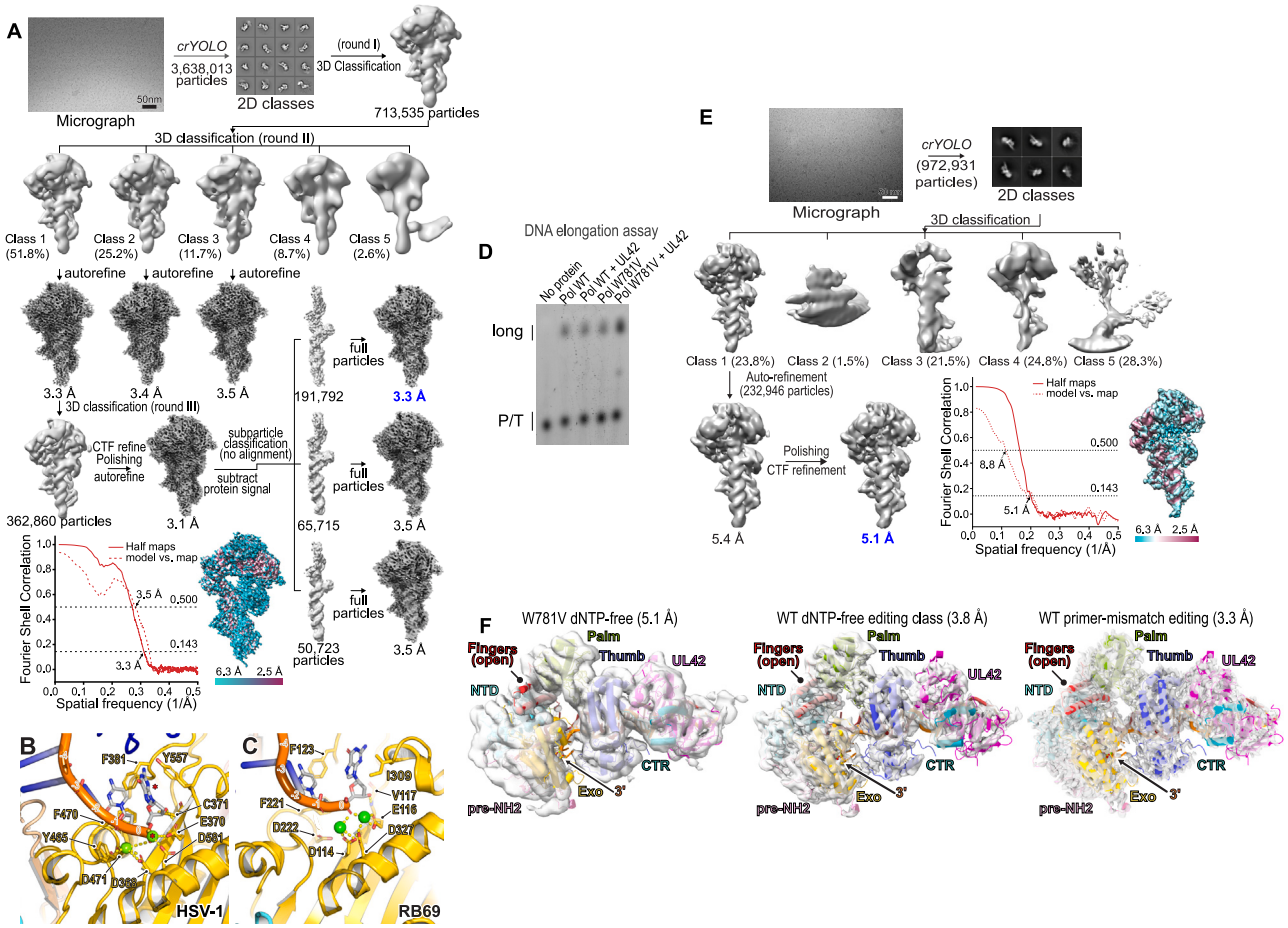

Figure S7. Structure determination of a mismatch-containing DNA primer-template-bound wild-type HSV polymerase in the editing conformation and of the W781V mutant polymerase, related to Figure 5

(A) Flow chart depicting cryo-EM data processing workflow for determining the structure of a mismatch-containing DNA primer-template-bound (PT3) wild-type (WT) HSV polymerase. The resolution of the map used for structural analysis is indicated in blue, and a Fourier shell correlation plot is provided for this map. Estimates of local resolution were determined using ResMap.[96] Additional information is provided in the STAR Methods.

(B) Exo active site in the DNA-bound WT HSV polymerase holoenzyme editing complex. Features for the terminal base and the metal that are labeled with an asterisk were associated with very weak density (likely because of flexibility and/or base excision) and are modeled here but not deposited in final coordinates.

(C) Exo active site configuration in the X-ray crystal structure of DNA-bound bacteriophage RB69 gp43 (Pol) in the editing conformation (PDB: 1CLQ).[51] The view is similar to that for the HSV polymerase Exo active site shown in (B).

(D) Long-chain DNA synthesis by WT or W781V mutant HSV Pol in the absence or presence of UL42. Reactions were visualized by using a fluorescein-labeled primer followed by electrophoresis on a DNA sequencing gel and imaging with a scanner.

(E) Flow chart depicting cryo-EM data processing workflow for determining the structure of the DNA primer-template-bound (PT1) W781V HSV polymerase holoenzyme without nucleotide. The resolution of the map that was used for coordinate docking is indicated in blue, and Fourier shell correlation plots are provided for this map. Estimates of local resolution were determined using ResMap.[96] Additional information is provided in the STAR Methods.

(F) Docking of the atomic coordinates for the mismatch-containing DNA primer-template editing structure into the 5.1 Å map of the HSV mutant polymerase holoenzyme in the absence of dTTP (left). For comparison, docking was also performed for the editing class of the WT enzyme observed in the absence of dNTP (middle). The WT editing polymerase bound to mismatch-containing DNA primer-template and corresponding 3.3 Å map are also shown for comparison (right). See also Video S3.